

# Concentration and Length Dependence of DNA Looping in Transcriptional Regulation

Lin Han<sup>1</sup>, Hernan G. Garcia<sup>2</sup>, Seth Blumberg<sup>1</sup>, Kevin B. Towles<sup>3</sup>,  
John F. Beausang<sup>3</sup>, Philip C. Nelson<sup>3</sup>, Rob Phillips<sup>1\*</sup>

<sup>1</sup>Department of Applied Physics, California Institute of  
Technology, Pasadena CA 91125;

<sup>2</sup>Department of Physics, California Institute of  
Technology, Pasadena CA 91125;

<sup>3</sup>Department of Physics and Astronomy, University of Pennsylvania,  
Philadelphia PA 19104

\*Corresponding author: [phillips@pboc.caltech.edu](mailto:phillips@pboc.caltech.edu)

July 8, 2021

## Abstract

**BACKGROUND.** In many cases, transcriptional regulation involves the binding of transcription factors at sites on the DNA that are not immediately adjacent to the promoter of interest. This action at a distance is often mediated by the formation of DNA loops: Binding at two or more sites on the DNA results in the formation of a loop, which can bring the transcription factor into the immediate neighborhood of the relevant promoter. These processes are important in settings ranging from the historic bacterial examples (bacterial metabolism and the lytic-lysogeny decision in bacteriophage), to the modern concept of gene regulation to regulatory processes central to pattern formation during development of multicellular organisms.

**METHODOLOGY/PRINCIPAL FINDINGS.** Though there have been a variety of insights into the combinatorial aspects of transcriptional control, the mechanism of DNA looping as an agent of combinatorial control in both prokaryotes and eukaryotes remains unclear. We use single-molecule techniques to dissect DNA looping in the *lac* operon. In particular, we measure the propensity for DNA looping by the Lac repressor as a function of the concentration of repressor protein and as a function of the distance between repressor binding sites.

**CONCLUSIONS/SIGNIFICANCE.** As with earlier single-molecule studies, we find (at least) two distinct looped states and demonstrate that the presence of these two states depends both upon the concentration of repressor protein and the distance between the two repressor binding sites. We find that loops form even at interoperator spacings considerably shorter than the DNA persistence length, without the intervention of any other proteins to prebend the DNA. The concentration measurements also permit us to use a simple statistical mechanical model of DNA loop

formation to determine the free energy of DNA looping, or equivalently, the  $J$ -factor for looping.

# 1 Introduction

The biological significance of DNA is primarily attributed to the information implicit in its sequence. Still, there are a wide range of processes for which DNA's physical basis as a stiff polymer also matters [1]. For example, the packaging of DNA into nucleosomes appears to select for sequence motifs that are particularly flexible [2, 3]. In the setting of transcriptional regulation, there are a host of regulatory architectures both in prokaryotes and eukaryotes which require the interaction of sequences on the DNA that are not adjacent [4, 5, 6, 7]. These interactions are mediated by DNA-binding proteins, which have to deform the DNA. Of late, it has become possible to perform genome-wide surveys to determine the entirety of looped configurations induced by a given protein [8, 9]. In eukaryotes, action of transcription factors over long distances seems the rule rather than the exception. One of the most transparent examples of DNA looping is in bacteria where some repressors and activators can bind at two sites simultaneously, resulting in a DNA loop. This effect was first elucidated in the context of the arabinose operon [10]. It is an amusing twist of history that the two regulatory motifs considered by Jacob and Monod, namely, the switch that makes the decision between the lytic and lysogenic pathways after phage infection [11] and the decision making apparatus associated with lactose digestion in bacteria [5, 12], both involve DNA looping as well.

To understand the physical mechanism of the biological action at a distance revealed by DNA looping, it is necessary to bring both *in vitro* and *in vivo* experiments as well as theoretical analyses to bear on this important problem. Over the last few decades there have been a series of impressive and beautiful experiments from many quarters that inspired our own work. In the *in vivo* context, it is especially the work of Müller-Hill and coworkers that demonstrates the intriguing quantitative implications of DNA looping for regulation [13]. In their experiments, they tuned the length of the DNA loop in one base pair increments and measured the resulting repression. More recently, these experiments have been performed with mutant bacterial strains that were deficient in architectural proteins such as HU, IHF and H-NS [14, 15]. On the *in vitro* side, single molecule experiments using the tethered-particle method [16, 17, 18, 19, 20, 21, 22, 23, 24] have also contributed significantly [25, 26, 27, 28, 29, 30]. The idea of these experiments is to tether a piece of DNA to a microscope cover slip with a bead attached to the end. The DNA construct has the relevant binding sites (operators) for the protein of interest along the DNA and when one of these proteins binds, it shortens the length of the tether. As a result of the shorter tether, the Brownian motion of the bead is reduced. Hence, the size of the random excursions of the bead serves as a reporter for the status of the DNA molecule (i.e. looped or unlooped, DNA-binding protein present or not).

In addition to single-molecule studies, *in vitro* biochemical assays have also shed important light on the interactions between transcription factors and their DNA targets. Both filter binding assays and electrophoretic mobility shift assays have been widely used to study how variables dictating DNA mechanics such as length and degree of supercoiling, alter the looping process [31, 32, 33, 34, 35].

One of the missing links in the experimental elucidation of these problems is systematic, single-molecule experiments which probe the length, repressor concentration and sequence dependence of DNA looping. Such experiments will complement earlier *in vivo* work, which has already demonstrated how DNA length and repressor concentration alter repression [13]. Our view is that such systematic experiments will help clarify the way in which both length and sequence contribute to the probability of DNA looping, and begin to elucidate the mechanisms whereby transcription factors act over long genomic distances. Further, such experiments can begin to shed light on broader questions of regulatory architecture and the significance of operator placement to transcriptional control. To that end, we have carried out experiments that probe the DNA looping process over a range of concentrations of repressor protein and for a series of different loop lengths. In addition, intrigued by the sequence preferences observed in nucleosomal DNA, we have made looping constructs in which these highly bendable nucleosomal sequences are taken out of their natural eukaryotic context and are inserted between the operators that serve as binding sites for the Lac repressor (the results of those experiments will be reported elsewhere). The point of this exercise is to see how the looping probability depends upon these tunable parameters, namely, length, repressor concentration and sequence.

Our key results are: (1) The concentration dependence of looping as a function of repressor concentration (a “titration” curve) can be described by a simple equilibrium statistical-mechanics model of transcription factor-DNA interactions. The model predicts a saturation effect, which agrees with our experimental observations. (2) By measuring this effect, we were able to isolate the free energy change of looping (that is, separate it from the binding free energy change), obtaining an experimental measurement of its value for a range of different lengths in an uncluttered, *in vitro*, setting. (3) Systematic measurement of looping free energy as a function of interoperator spacing hints at the same modulations seen in analogous *in vitro* work on cyclization [3, 36], and *in vivo* work on repression [13, 14]. (4) Clear experimental signature of multiple looped states, consistent with theory expectations [37, 38, 39, 40] and other recent experiments [28, 30]. In the remainder of the paper, we describe a series of experiments that examine both the length and concentration dependence of DNA looping induced by the Lac repressor. A companion paper gives extensive details about our theoretical calculations [41].

## 2 Results

As argued above, one of our central concerns in performing these experiments was to have sufficient, systematic data to make it possible to carry out a thorough analysis of the interplay between theories of transcriptional regulation (and DNA looping) [42, 43, 44, 45], and experiment. To that end, we have carried out a series of DNA looping experiments using the tethered-particle method [25] for loop lengths ranging from 300 to 310 bp in one base pair increments as well as several representative examples for lengths below 100 bp. The experiments described here use DNA constructs harboring two different operators, symmetric operator *Oid* and primary natural operator *O1* as Lac repressor binding sites. In addition, we have explored how the looping trajectories depend upon the concentration of Lac repressor. The particular experimental details are described in the “Materials and Methods” section.

A typical experimental trace resulting from these measurements is shown in fig. 1. (Representative examples of experimental traces from all of the lengths and concentrations considered throughout the paper as well as examples of rejected traces are shown in the Supplementary Material.) As seen in the figure, as with other recent work [28, 30], there are clearly two distinct looped states as seen both in the trajectory and the histogram. Control experiments with one of the two binding sites removed show only the highest peak, which further supports the idea that the two lower peaks indeed indicate looped configurations. One hypothesis is that these two looped states correspond to two different configurations of the Lac repressor molecule and its attendant DNA, which we will refer to as the “open” and “closed” configurations. Direct interconversion between the two looped species suggested the two distinct looped states are indeed due to different conformations of Lac repressor protein [28]. An alternate hypothesis is that the two peaks reflect different DNA topologies [47, 48, 49]. Although this hypothesis does not obviously accommodate the apparent observation of direct interconversion, nevertheless we will present data from Monte Carlo simulations of DNA chain conformations that show that it *can* quantitatively explain the observed multi-peak structure observed in the data.

### 2.1 Concentration dependence

In order to extract quantities such as the free energy of looping associated with repressor binding (or equivalently, a *J*-factor for looping) and to examine how the propensity for looping depends upon the number of repressors, we needed looping data at a number of different concentrations. At very low concentration, we expect that there will be negligible looping because neither of the operators will be bound by Lac repressor. At intermediate concentrations, the equilibrium will be dominated by states in which a single repressor

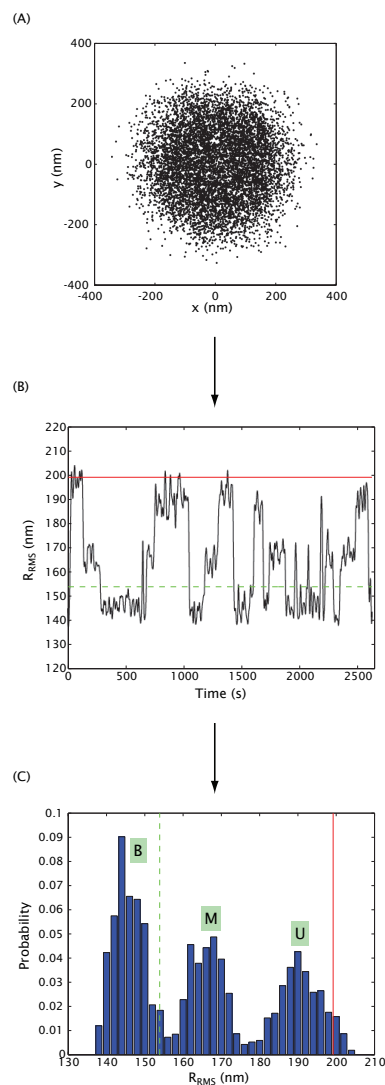


Figure 1: Different representations of TPM data. (A) Scatter plot of drift-corrected positional data. Each dot corresponds to the instantaneous projected position of the bead at a particular instant in time. (B) Running average of Gaussian filtered RMS motion over an effective window of 4 seconds.  $R$  is the distance from the bead center (dots in panel (A)) to the tether attachment point (centroid of all dots in panel (A)). Red (solid) and green (dashed) lines represent naively expected motion, based on calibration measurements [46], for 901bp DNA and an imagined DNA for which 305+20.5 bp (the center to center distance between operators) are subtracted off of the full length 901 bp tether. (Fig. 10 gives a more precise prediction of the expected excursions in looped states.) (C) Histogram of the RMS motion. Different peaks correspond to looped (labeled B, bottom, and M, middle) or unlooped (labeled U) states. The DNA used here is pUC305L1 (see Materials and Methods section) with 100 pM Lac repressor. A detailed discussion of how to go from microscopy images of beads to traces and histograms like those shown here is given in the Supplementary Materials.

tetramer is bound to the DNA at the strong operator, punctuated by transient looping events. In the very high concentration limit, each operator will be occupied by a tetramer (see fig. 4 below), making the formation of a loop nearly impossible.

This progression of qualitative behavior is indeed seen in fig. 2, which shows data from eight distinct concentrations of Lac repressor, as well as a single-operator control in which the DNA lacks a secondary operator. Throughout this work we define *sequence length* or *loop length* as the end-to-end distance between the operators as shown in fig. 14. These curves correspond to a sequence length of 306 bp and are generated by summing the normalized histograms from *all* of the individual trajectories for each concentration that pass our bead selection criteria (bead selection criteria are discussed in detail in the Supplementary Materials). A key feature of these data is the way in which the two looped states are turned off as the concentration of Lac repressor is increased to very high levels. This phenomenon is expected since the Lac repressor exists always as tetramers under the conditions used here [50, 51], and competition for binding at the second operator between loose Lac repressor and Lac repressor bound to the other operator is stronger as the concentration of Lac repressor increases. However, the two different looped species have slightly different responses at high repressor concentrations. For example, at 1 nM concentrations, the intermediate looped state has become very infrequent, whereas the shortest looped state remains competitive. Similar concentration dependence of Lac repressor mediated DNA looping was studied previously [26] at 4 pM, 20 pM and 100 pM. Those experiments revealed that looping is suppressed as the concentration goes up.

One way to characterize the looping probability as a function of concentration is shown in fig. 3. There are various ways to obtain data of the sort displayed in this plot. First, by examining the trajectories, we can simply compute the fraction of time that the DNA spends in each of the different states, with the looping probability given by the ratio of the time spent in either of the looped states to the total elapsed time. Of course, to compute the time spent in each state, we have to make a thresholding decision about when each transition has occurred. This can be ambiguous, because trajectories sometimes undergo rapid jumps back and forth between different states; it is not unequivocally clear when an apparent transition is real, and when it is a random fluctuation without change of looping state. A second way of obtaining the looping probability is to use fig. 2 and to compute the areas under the different peaks and to use the ratios of areas as a measure of looping probability. This method, however, does not properly account for possible variation between different beads, because they are all added up into one histogram. A third alternative is to obtain the looping probability for each *individual* bead, by plotting its histogram and calculating the area under that subset of the histogram corresponding to the looped states. We used this last method to calculate the mean looping probability

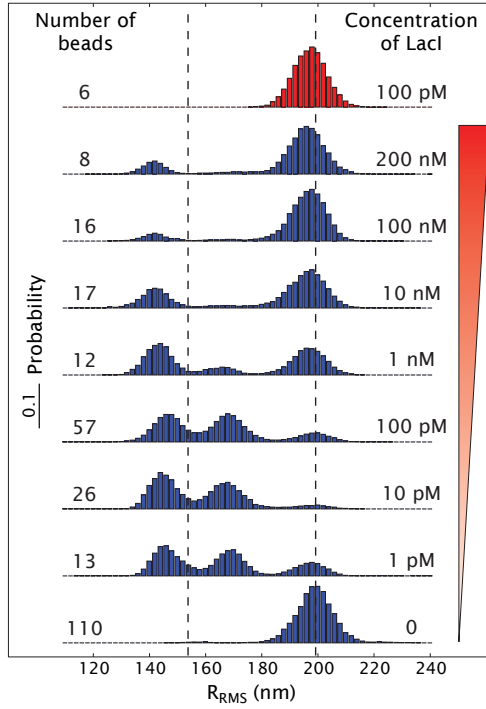


Figure 2: Concentration dependence of the distribution of bead excursions. The histograms show the distribution of RMS motions averaged over 4 seconds at different concentrations of Lac repressor. The blue histograms correspond to measurements for a length between operators of  $L_{\text{loop}} = 306$  bp (see fig. 14), whereas the red histogram is a control where  $O1$  has been deleted. The two dashed lines represent the naively expected motion, based on our calibration measurements [46]. (See fig. 10 for a more precise prediction of the peak locations.) Representative single-molecule trajectories resulting in these histograms are shown in the Supplementary Material.



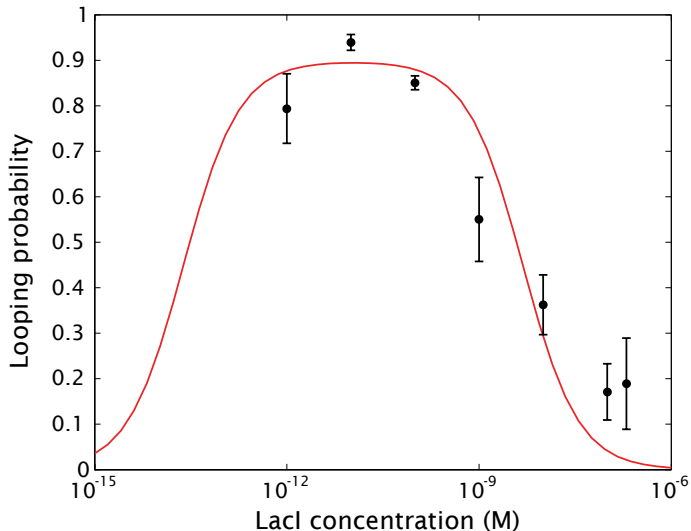


Figure 3: Looping probability  $p_{\text{loop}}$ , at different concentration of Lac repressor. The DNA used in these experiments is 901 bp long and the loop length is  $L_{\text{loop}} = 306$  bp. The vertical axis gives looping probability (fraction of time spent in either of the two looped states). The fraction of time spent in the looped states was calculated for each bead individually and the mean and standard error calculated for each construct. The curve is a fit to the experimental data using the statistical mechanics model described in the text.

and the standard error for each construct, which is shown in fig. 3.

These results can also be explored from a theoretical perspective using the tools of statistical mechanics [44, 45, 52]. The goal of a statistical mechanical description of this system is to compute the probability of the various microstates available to the repressor-DNA system as shown in fig. 4. The simplest model posits 5 distinct states [25, 26, 28]: Both operators empty,  $Oid$  occupied by repressor without looping,  $O1$  occupied by repressor without looping,  $Oid$  and  $O1$  separately occupied by single repressors and the looped state (the subtleties associated with the statistical weight of the looped state are described in the Supplementary Materials). The model does not take into account the effect of non specific binding of Lac repressor to non-operator DNA, because a simple estimate reveals that the vast majority of repressors are free in solution rather than bound nonspecifically to the tethered DNA. We argue that this effect is negligible because the equilibrium association constant of Lac repressor to non-operator DNA at conditions similar to ours is around  $10^6 \sim 10^7 \text{ M}^{-1}$  [53, 54, 55, 56, 57, 58, 59], which is roughly six orders of magnitude less

than the corresponding quantity for specific binding [32, 60, 61, 62, 63, 64, 65]. Given such association constants, the ratio between non specifically bound Lac repressor and the free Lac repressor in solution is given as

$$\begin{aligned}\frac{[RD]}{[R]} &= K_{NS} \times [D] \\ &\approx 2 \times 10^{-5},\end{aligned}$$

where  $[RD]$  is the concentration of non-specifically bound Lac repressor,  $[R]$  is the concentration of Lac repressor in solution, and  $[D]$  is the DNA concentration, which is around 2 pM in our experiment. For  $[R] = 200$  nM, we have  $[RD] \approx 4$  pM, which is far smaller than the concentration of Lac repressor in solution.

It is convenient to describe the probability of the various states using both the language of microscopic binding energies (and looping free energies) and the language of equilibrium constants (and  $J$ -factors). From a microscopic perspective, the key parameters that show up in the model are the standard free energy changes for repressor binding to the two operators,  $\Delta\epsilon_{id}$  and  $\Delta\epsilon_1$ , the looping free energy  $\Delta F_{loop}$  and the concentration of repressor  $[R]$ . The binding energy here contains two components. One is the standard positional free energy required for bringing one Lac repressor molecule to its DNA binding site at 1 M concentration of Lac repressor. The other is the rotational entropy loss times  $-T$ , plus the interaction free energy due to the physical contact upon protein binding [44, 45, 66]. The associated free energy with each configuration gives the statistical weights of the equilibrium probability (listed in the middle column of fig. 4). For example, to obtain the probability of the looped state, we construct the ratio of state (v) in the figure to the sum over all five states, as given by

$$\begin{aligned}p_{loop} &= \left[ 8 \frac{[R]}{1 \text{ M}} e^{-\beta(\Delta\epsilon_1 + \Delta\epsilon_{id} + \Delta F_{loop})} \right] \\ &\quad \left[ 1 + 4 \frac{[R]}{1 \text{ M}} \left( e^{-\beta\Delta\epsilon_1} + e^{-\beta\Delta\epsilon_{id}} \right) + 16 \left( \frac{[R]}{1 \text{ M}} \right)^2 e^{-\beta(\Delta\epsilon_1 + \Delta\epsilon_{id})} + \right. \\ &\quad \left. 8 \frac{[R]}{1 \text{ M}} e^{-\beta(\Delta\epsilon_1 + \Delta\epsilon_{id} + \Delta F_{loop})} \right]^{-1},\end{aligned}\tag{1}$$

where  $\beta = 1/k_B T$ . As detailed in the Supplementary Materials and can be read off from the right column in fig. 4, this microscopic description is conveniently rewritten in terms

of the equilibrium constants and  $J$ -factor for looping as

$$p_{\text{loop}} = \frac{\frac{1}{2} \frac{[R]J_{\text{loop}}}{K_1 K_{id}}}{1 + \frac{[R]}{K_1} + \frac{[R]}{K_{id}} + \frac{[R]^2}{K_1 K_{id}} + \frac{1}{2} \frac{[R]J_{\text{loop}}}{K_1 K_{id}}}. \quad (2)$$

Here  $J_{\text{loop}}$  is the average of the individual  $J$  factors corresponding to different loop topologies. These topologies can be classified according to the orientation of each one of the operators with respect to the binding heads. We define the state variables  $\alpha$  and  $\beta$  that describe the orientation of  $O1$  and  $Oid$ , respectively, and that can adopt a value of either 1 or 2. The average  $J_{\text{loop}}$  is then

$$J_{\text{loop}} = \frac{1}{4} \sum_{\alpha, \beta} J_{\text{loop}, \alpha, \beta}. \quad (3)$$

An alternative to this scheme is to construct the ratio  $p_{\text{unloop}}/p_{\text{loop}}$ . In the limit where the strongest operator,  $Oid$ , is always occupied, this ratio takes the simple, linear form

$$p_{\text{ratio}} = \frac{2K_1}{J_{\text{loop}}} + \frac{2[R]}{J_{\text{loop}}}. \quad (4)$$

This permits the determination of the  $J$ -factor as the slope of a linear fit of the form without necessarily a need to obtain  $K_1$ . Below we discuss the validity of this particular model. For the remaining data points at loop lengths other than 306 bp, where no titration was done, we can use the relation

$$J_{\text{loop}}(L) = \frac{p_{\text{ratio}}(306 \text{ bp})}{p_{\text{ratio}}(L)} J_{\text{loop}}(306 \text{ bp}). \quad (5)$$

Just like in the titration case, this relation allows to obtain  $J_{\text{loop}}$  without knowing  $K_1$ , as long as we know at least one value of  $J_{\text{loop}}$  and its corresponding  $p_{\text{ratio}}$ .

The data shown in fig. 3 can be fit in several different ways as suggested by the three different formulae characterizing the looping probability given above. The fit shown in fig. 3 is a full nonlinear fit in which the parameters  $K_1$ ,  $K_2$  and  $J_{\text{loop}}$  are treated as fitting parameters. Alternatively, using this same data of fig. 3, we can actually obtain the looping free energy, as well as the binding energies by fitting the data to eqn. 1. Finally, we can fit the data corresponding to LacI concentrations of 10 pM and higher using the linear model from eqn. 4. The results of these different fits are shown in Table 1. These results are usefully contrasted with results of other experiments on the *lac* operon, which are also summarized in Table 1. We see from the table that the nonlinear model fails to constrain

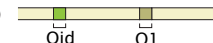
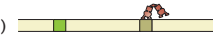

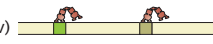

STATE	WEIGHT	
	STATISTICAL MECHANICS	THERMODYNAMICS
(i) 	1	1
(ii) 	$4 \frac{[R]}{1M} e^{-\Delta\varepsilon_1/k_B T}$	$\frac{[R]}{K_1}$
(iii) 	$4 \frac{[R]}{1M} e^{-\Delta\varepsilon_{id}/k_B T}$	$\frac{[R]}{K_{id}}$
(iv) 	$16 \left(\frac{[R]}{1M}\right)^2 e^{-(\Delta\varepsilon_1 + \Delta\varepsilon_{id})/k_B T}$	$\frac{[R]}{K_1} \frac{[R]}{K_{id}}$
(v) 	$8 \frac{[R]}{1M} e^{-(\Delta\varepsilon_1 + \Delta\varepsilon_{id} + \Delta F_{loop})/k_B T}$	$\frac{1}{2} \frac{[R]}{K_1} \frac{J_{loop}}{K_{id}}$

Figure 4: States and weights for the Lac repressor-DNA system [44]. Each of the five state classes shown in the left column has a corresponding statistical weight given by the product of the Boltzmann factor and the microscopic degeneracy of the state. All of the weights have been normalized by the weight of the state in which the DNA is unoccupied. State (v) is treated as a single looped state, even though there are multiple distinct looped configurations. The third column shows how to write these statistical weights in the language of equilibrium constants and  $J$ -factors. The derivation of these weights and the relation between the statistical mechanical and thermodynamic perspectives can be found in the Supplementary Materials.

Parameter	Nonlinear fit	Linear fit	Literature value
$J_{\text{loop}}$	$8.6 \pm 6.3 \text{ nM}$	$52 \pm 40 \text{ nM}$	See fig. 11
$\Delta F_{\text{loop}}$	$18.6 \pm 0.7 k_B T$	$16.8 \pm 0.8 k_B T$	N/A
$K_1$	$0.49 \pm 0.45 \text{ nM}$	$3.0 \pm 2.5 \text{ nM}$	10 $\sim$ 22 pM [32, 60, 61, 62, 63, 64, 65]
$\Delta \varepsilon_1$	$-20.0 \pm 0.9 k_B T$	$-18.2 \pm 0.8 k_B T$	$-23.2 \sim -24.0 k_B T$
$K_{id}$	$0.2 \pm 2.3 \text{ pM}$	N/A	2.4 $\sim$ 8.3 pM [67]
$\Delta \varepsilon_{id}$	$-28 \pm 9 k_B T$	N/A	$-24.1 \sim -25.4 k_B T$

Table 1: Results from the LacI titration experiments. The probability of looping as a function of Lac repressor concentration shown in fig. 3 was fitted to the two non-linear models from eqns. 18 and 20. A subset of the data corresponding to concentrations of LacI 10 pM and higher is fitted to the linear model shown in eqn. 4 and its statistical mechanics counterpart. The literature values correspond to bulk binding assays performed in concentration ranges close to our TPM buffer conditions.

the value of  $K_{id}$  reliably. In the case of the  $O1$  binding constants we see a difference of almost two orders of magnitude with published dissociation constants, which translates into a difference of roughly  $4 k_B T$  in the binding energy.

One of the challenges of single-molecule experiments like those described here is that the concentration of protein introduced into the system may not correspond to the actual concentration “seen” by the DNA that is tethered to the surface. For example, some of the protein might be lost as a result of nonspecific binding to the microscope cover slip. From the linear model shown in eqn. 4 it follows that any error in the concentration will translate linearly into an error in  $J_{\text{loop}}$  and  $K_1$ . Therefore, in order for the above discrepancy to be explained solely by surface effects on the LacI concentration we would have to have a difference of between one and two orders of magnitude between the concentration of the stock that flowed into the chamber and the actual free concentration inside of it.

Once the parameters that characterize the model are in hand, we can plot the probability of all five possible states as a function of the Lac repressor concentration as shown in fig. 5. This figure reveals that at the concentrations we normally use ( $[R] = 100 \text{ pM}$ ), the system is dominated by the looped state and the state with single occupancy of  $O_{id}$ . A detailed discussion of the significance of the looping free energies (or the  $J$ -factors) will follow later in the paper once we have explored the question of the length dependence of DNA looping in the *lac* operon.

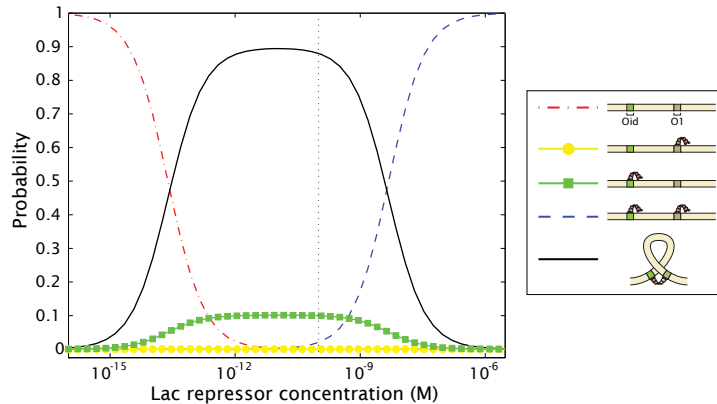


Figure 5: Probabilities for different states of Lac repressor and operator DNA. The curves show the probabilities of the five classes of microscopic states used in the statistical mechanics model based upon parameters shown in table 1. The vertical line corresponds to the concentration at which the loop length experiments in the remainder of the paper are performed.

## 2.2 Length dependence

### 2.2.1 1bp resolution for a whole helical turn: $L_{\text{loop}} = 300$ bp to 310 bp

The beautiful *in vivo* repression experiments of [13] demonstrate that the length of the DNA loop formed by Lac repressor strongly affects the probability of loop formation (especially for loop lengths less than 150 bp). In particular, those authors (and others) [14, 15, 68, 69] have observed “phasing”: The relative orientations of the two operators changes the ease with which repressor can bind. Similar phasing effects have been observed in *in vitro* cyclization assays [3, 36, 70, 71]. What has not been clear is how to concretely and quantitatively relate these results on DNA mechanics from the *in vivo* and *in vitro* settings and how to use such insights to better understand the interplay between the physical and informational properties of DNA *in vivo*. Our idea was to systematically examine the same progression of DNA lengths that have been observed *in vivo*, but now using TPM experiments. To that end, we have measured TPM trajectories for a series of interoperator spacings measured in 1 bp increments. The results of this systematic series of measurements for DNAs harboring operators spaced over the range  $L_{\text{loop}} = 300 \sim 310$  bp are shown in fig. 6 (as are the results for several shorter lengths to be discussed in the next section). Each plot shows the probability of the three states for a particular interoperator spacing.

The data can be converted into a plot of the dependence of the looping probability on interoperator spacing as shown in fig. 7. This figure shows  $p_{\text{loop}}$  as a function of the DNA

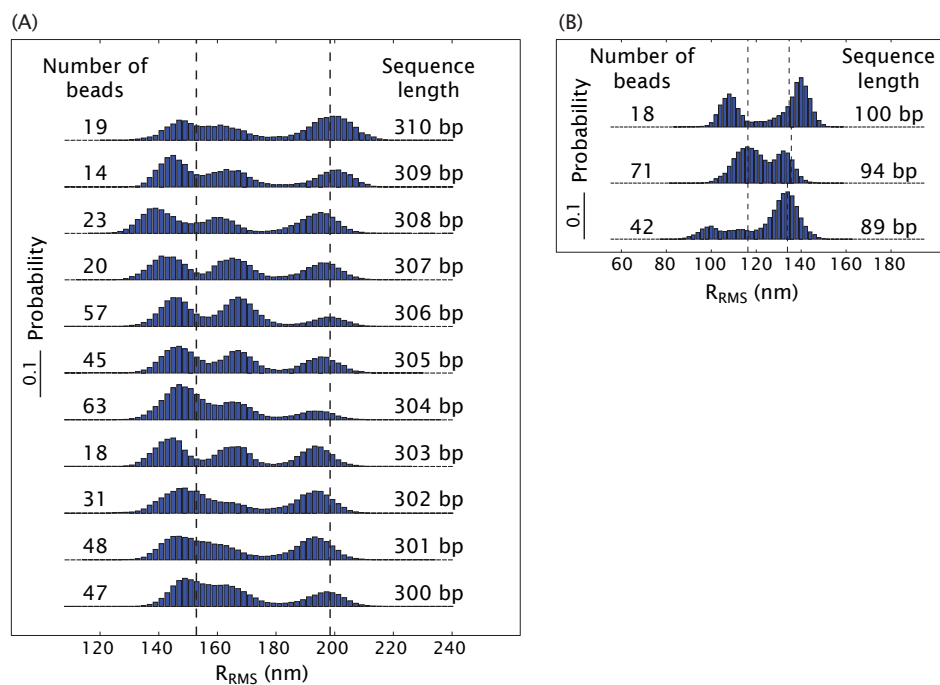


Figure 6: Length dependence of DNA looping. (A) Histogram of the tethered Brownian motion for DNAs with two Lac repressor binding sites spaced from  $L_{loop} = 300$  bp (bottom) to 310 bp (top). (B) Histogram of the Brownian motion for DNAs with two Lac repressor binding sites spaced at  $L_{loop} = 89$ , 94 and 100 bp. The two dashed lines represent the naively expected motion based on our calibration measurements for the full length tether and the same DNA when the center to center distance between operators is subtracted from the tether length. (Again see also fig. 10.) Representative traces for each of the lengths shown here can be found in the Supplementary Material.

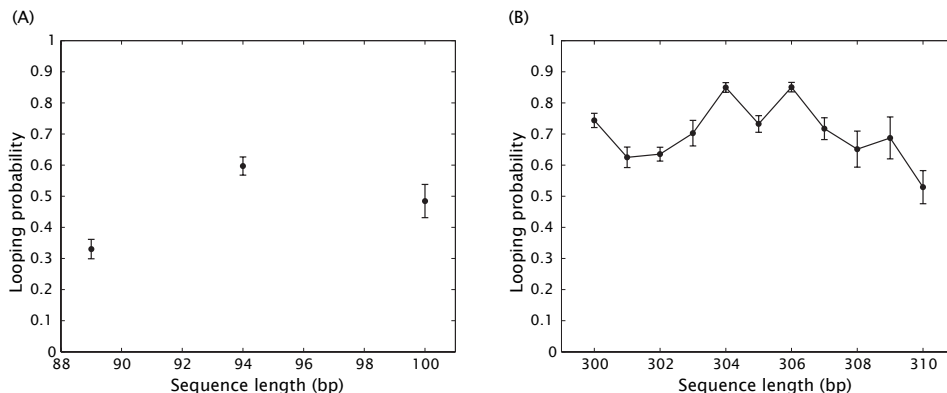


Figure 7: Looping probability  $p_{\text{loop}}$ , as a function of interoperator spacing. (A) Looping probability for short constructs. (B) Looping probability for one full helical repeat. These probabilities are obtained by averaging over the  $p_{\text{loop}}$  of each bead. The error bars correspond to the standard error associated with this magnitude. For more information see Supplementary Materials.

length between the two operators. The looping probability shows a weak dependence on the interoperator spacing but reveals no conclusive signature of phasing; to really detect such phasing with confidence, however, would require more measurements in single basepair increments. The maximum looping is achieved when the two binding sites are 306 bp apart, suggesting that at this distance, the two sites are in an optimal phasing orientation for binding of the two heads of Lac repressor. The ability to form stable out-of-phase (two binding sites are on the opposite side of the DNA) loops with only a small reduction in stability is consistent with previous studies [28]. The relatively stable looping over the entire helical repeat is also consistent with the relatively constant repression level *in vivo* for similar interoperator spacing [13].

As already indicated in Table 1, the looping probability can be converted into a corresponding looping free energy based on the statistical mechanics model described above and culminating in eqn. 1. The results of such calculation are shown in fig. 8. The measurements on length dependence permit us to go beyond the concentration dependence measurements by systematically exploring how the phasing of the two operators impacts the free energy of DNA looping. One might expect that when the two operators are on opposite sides of the DNA, additional twist deformation energy is required to bring the operators into good registry for Lac repressor binding. Our results show that the phasing effect imposes an energy penalty  $\Delta F_{\text{loop}}$  that differs by only about  $1.5 k_B T$  between the in-phase and out of phase cases. An alternative interpretation of these same results on



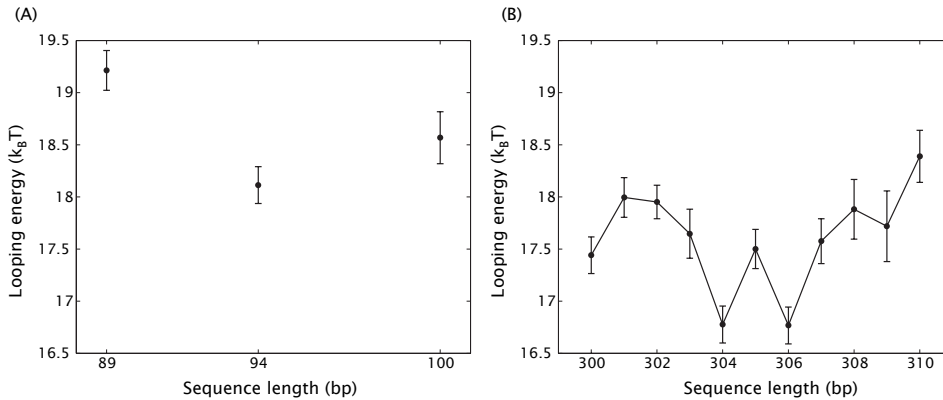


Figure 8: Length dependence of free energy of looping, defined via eqn. 1 with choice of reference concentration 1 M. (A) Looping free energy for short constructs. (B) Looping free energy for a full helical repeat.

looping probability is offered by the  $J$ -factor for looping as shown in fig. 9.

To get a feel for the energy scale associated with twist deformations, we perform a simple estimate. Twisting DNA for a torsional angle  $\theta$  requires energy

$$\Delta F_t = k_B T \xi_{tp} \theta^2 / 2L \quad (6)$$

where  $\xi_{tp}$  is the torsional persistence length for double stranded DNA, which is around 250 bp [72, 73, 74].  $L$  is the DNA length. For half a helical turn twist,  $\theta = \pi$  and  $L = 300$  bp. The energy introduced for half a helical turn is around  $4.11 k_B T$ . Our experimentally determined looping energy difference between in-phase and out-of-phase DNA, about  $1.5 k_B T$ , is indeed comparable in magnitude to this estimate. Our simple estimate is somewhat high, in part because it neglects the fact that in addition to twisting, a loop can writhe to accommodate a nonideal operator phasing. Additionally, the observed small magnitude of our observed phasing modulation may reflect partially canceling out-of-phase contributions of different topologies [41], not a low free energy cost for twisting. Finally, the Lac repressor itself is flexible, and so can partially compensate for nonideal phasing.

### 2.2.2 Sub-persistence length loops

One of the intriguing facts about the architecture of regulatory motifs that involve DNA looping is that often the loops formed in these systems have DNA lengths that are con-

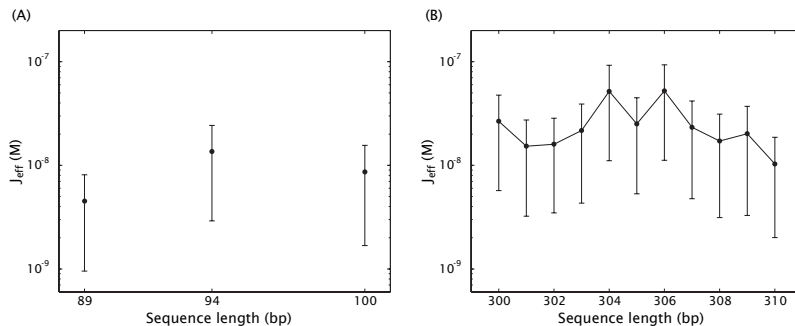


Figure 9: Looping  $J$ -factor resulting from TPM measurements. (A) Effective  $J$ -factor for looping resulting from TPM data on short constructs. (B) Effective  $J$ -factor for looping resulting from TPM data on a full helical repeat.

siderably shorter than the persistence length of DNA (i.e. 150 bp). For example, in the *lac* operon, one of the two wild-type loops has a length of 92 bp. However, this trend goes well beyond the *lac* operon as is seen for a variety of different architectures found in *E. coli*, for example [1]. As a result, it is of great interest to understand the interplay between transcriptional regulation and corresponding mechanical manipulations of DNA this implies.

So far, we have considered loops that are roughly two-fold larger than the persistence length through our investigation of one full helical repeat between 300 and 310 bp. To begin to develop intuition for the mechanism of loop formation in the extremely short loops exhibited in many regulatory architectures, we have examined three different lengths: 89, 94 and 100 bp. One of the reasons that the examination of these loops is especially important is that it has been speculated that the *in vivo* formation of these loops either requires special supercoiling of the DNA or the assistance of helper proteins that prebend the DNA [1]. However, as indicated by the TPM results shown in fig. 6(B), even in our controlled *in vitro* setting, where neither of these mechanisms can act, Lac repressor is nevertheless able to form DNA loops. The essence of these experiments is identical to those described earlier in the paper except that now the overall tether lengths are shorter so as to ensure that the loops are detectable. (Representative TPM trajectories for these lengths are shown in the Supplementary Material.) It is clear from the histograms that of the three lengths we have investigated, loop formation is most favorable at 94 bp. Interestingly, it also appears that different loops are being formed for the in-phase and out-of-phase cases as evidenced by the changes of relative strengths among the looping peaks for the different constructs. The looping free energy and  $J$ -factor for looping for these short constructs are shown in

figs. 8(A) and 9(A).

### 2.3 Analysis of the TPM Experiment

Both the observed length and sequence dependence of the formation of a repression complex are intriguing from the perspective of DNA mechanics. In particular, DNA is not a passive mechanical bystander in the process of transcriptional regulation. To better understand the experiments carried out here and how they might shed light on the interplay of transcription factors and their target DNA, we have appealed to two classes of models: i) statistical mechanics models of the probability of DNA-repressor complex formation which depends upon the looping free energy (these models were invoked earlier in the paper to determine the looping free energy) and ii) Monte Carlo simulations of the TPM experiment itself which include the energetics of the bent DNA and excluded volume interactions of the bead with the cover slip. Our Monte Carlo calculations allow us to compute how easily loops form, based on a mathematical model of DNA elasticity. For illustration, we have chosen a linear-elasticity model, that is, a model in the class containing the wormlike chain, but any other elastic theory of interest can be used with the same calculation strategy. Details of these calculations appear in [41].

One of the puzzles that has so far been unresolved concerning DNA mechanics at short scales is whether *in vivo* and *in vitro* experiments tell a different story. In particular, *in vivo* experiments, in which repression of a given gene is measured as a function of the interoperator spacing [13, 14], have the provocative feature that the maximum in repression (or equivalently the minimum in looping free energy) correspond to interoperator spacings that are shorter than the persistence length. Some speculate that this *in vivo* behavior results from the binding of helper proteins such as the architectural proteins HU, H-NS or IHF [1, 14, 15] or the control of DNA topology through the accumulation of twist. In the TPM measurements reported here, there are neither architectural proteins nor proteins that control the twist of the DNA. As a result, these experimental results serve as a jumping off point for a quantitative investigation of whether DNA at length scales shorter than the persistence length behaves more flexibly than expected on the basis of the wormlike chain model. To address this question, we performed a series of simulations of the probability of DNA looping for short, tethered DNAs like those described here using, a variant of the wormlike chain model to investigate the looping probability. Our theoretical model used *no fitting parameters*; the few parameters defining the model were obtained from other, non-TPM, experiments.

The fraction of time spent in the looped configuration is controlled by several competing effects. For example, suppose that a repressor tetramer is bound to the stronger opera-

tor, *Oid*. Shortening the interoperator spacing reduces the volume over which the other operator (*O1*) wanders relative to the second binding site on the repressor, increases the apparent local “concentration” of free operator in the neighborhood of that binding site, and hence enhances looping. But decreasing the interoperator spacing also has the opposite effect of discouraging looping, due to the larger elastic energy cost of forming a shorter loop. Moreover, a shorter overall DNA construct increases the entropic force exerted by bead–wall avoidance, again discouraging looping [75]. To see what our measurement of this looping equilibrium tells us, we therefore needed to calculate in some detail the expected local concentration of operator (the “looping  $J$  factor”) based on a particular mathematical model of DNA elasticity. We chose a harmonic-elasticity model (a generalization of the traditional wormlike chain model), to see if it could adequately explain our results, or if, on the contrary, some non-harmonic model (for example the one proposed in [76, 77]) might be indicated.

To perform the required calculation, we modified the Gaussian sampling method previously used in [75, 78, 79, 80] (see Sect. 5.6 and [41]). Our code generated many simulated DNA chains, applied steric constraints [75], and reported what fraction of accepted chain/bead configurations had the two operator sites at the correct relative position and orientation for binding to the tetramer, which was assumed to be rigidly fixed in the form seen in PDB structure 1LBG [81]. Once this fraction has been computed, it is straightforward to relate it to the looping  $J$  factor [41]. To generate the simulated chains, we assumed a linear (harmonic, or wormlike-chain type) elastic energy function at the junctions in a chain of finite elements. Our energy function accounted for the bend anisotropy and bend–roll coupling of DNA, and yielded a value for the persistence length  $\xi = 44$  nm appropriate for our experiment’s buffer conditions [82, 83]. Our model did not account for sequence dependence, but this simplification is appropriate for comparison to our experimental results, which used random-sequence DNA. The simulation treated the bead and the microscope slide as hard walls and accounted for bead–wall, bead–chain, and wall–chain avoidance; we did not consider any interactions involving the repressor tetramer other than binding.

The symmetry of each LacI dimer implies four energetically equivalent ways for the two operators to bind when forming a loop, and hence four topologically distinct loop configuration classes [37, 38, 39, 40, 41]. We first asked whether this multiplicity of looped states could explain the general structure of the excursion distributions seen in fig. 6. Accordingly, we made histograms of the distance between wall attachment point and bead center for our simulated chains. Fig. 10 shows a subset of the same experimental data seen in fig. 6, together with the simulation results. Although the correspondence is not perfect, it is clear that the simple physical model of looping outlined above can account for many features of the data, for example the locations of the looped peaks and their

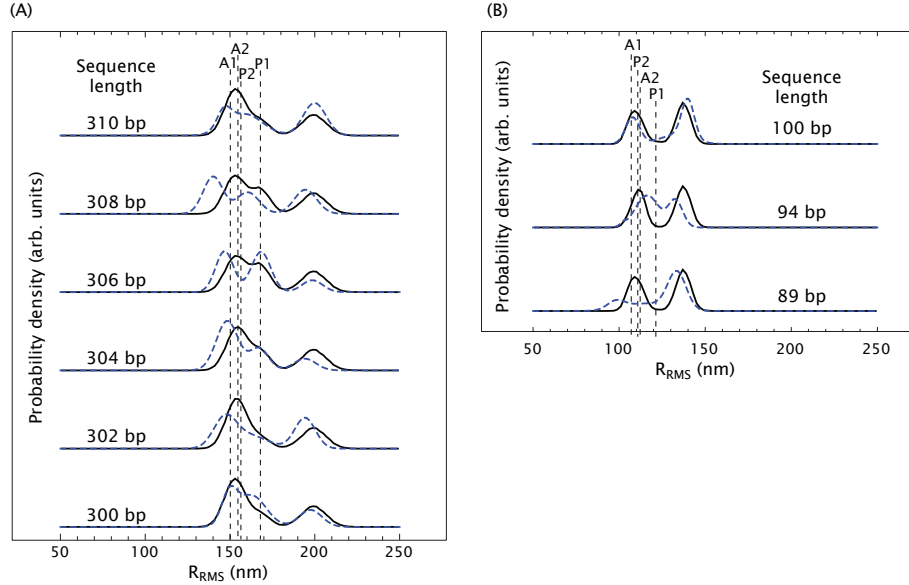


Figure 10: Theory and experiment for the probability density functions of RMS bead excursion for (A) our six “long chain” constructs and (B) our three “short chain” constructs. *Blue dashed curves* show the data in fig. 6, represented as sums of three Gaussians. *Black curves* show our theoretically predicted distributions. Because our simulation results were not fits to the data, they did not reproduce perfectly the ratio of looped to unlooped occupancies. For visualization, therefore, we have adjusted this overall ratio by a factor common to all six curves. This rescaling does not affect the locations of the peaks, the relative weights of the two looped-state peaks, nor the dependences of weights on loop length  $L_{\text{loop}}$ , all of which are zero-fit-parameter predictions of our model. The model yields these histograms as the sum of five contributions, corresponding to the four looped topologies and the unlooped state. The separate RMS displacements for each individual loop topology, for the 310 bp case in (A) and for the 100 bp case in (B), are also shown, labeled according to the scheme in [38].

relative strengths, including the variation as loop length is changed. We acknowledge that we have no definitive reply to the argument that the apparent direct transitions between the B and M peaks of our distributions seem to require an open-to-closed conformational switch in the tetramer [28]. We merely point out that the existence of three peaks in the distribution, with the the observed locations, is not by itself conclusive evidence of such a switch. (Indeed, Villa *et al.* have argued that the opening transition does not occur [84].)

We were also interested to see if the high incidence of looping observed in our experiments on short (sub persistence length) loops was compatible with the hypotheses above, or if on the contrary it demanded some modification to those hypotheses. Accordingly, we asked the simulation to compute the average  $J$  factor for loop lengths near 305 bp, and also for loop lengths near 95 bp. As discussed in ref. [41], the result of the simulation was that the ratio of these quantities is  $\bar{J}_{\text{loop}}(95 \text{ bp})/\bar{J}_{\text{loop}}(305 \text{ bp}) \approx 0.02$ . In contrast, fig. 9 shows that the experimental ratio is  $\approx 0.35 \pm 0.1$ , roughly 20-fold larger than the theoretical value. Our experimental results and those of our MC calculations for  $\bar{J}_{\text{loop}}$  as a function of loop length are shown in fig. 11.

We conclude that the hypotheses of linear elasticity, a rigid protein coupler, and no nonspecific DNA–repressor interactions, cannot explain the high looping incidence seen in our experiments. (Special DNA sequences loop even more easily than the random sequences reported here.) One possible explanation, for which other support has been growing, is the hypothesis of DNA elastic breakdown at high curvature [76, 77, 85]. An alternative hypothesis is that for our shorter loops, *both* the lower and the intermediate peaks in our distributions of bead excursion correspond to the some alternative, “open” conformation of the repressor tetramer [37, 38, 48, 86, 87, 88, 89]. To be successful, however, this hypothesis would have to pass the same quantitative hurdles to which we subjected our hypotheses. It would be very useful for future TPM experiments to instead examine other DNA-binding proteins known to be less flexible than LacI.

### 3 Discussion

The regulatory regions on DNA can often be as large as (or even larger than) the genes they control. The relation between the biological mechanisms of transcriptional control and the physical constraints put on these mechanisms as a result of the mechanical properties of the DNA remains unclear. One avenue for clarifying action at a distance by transcription factors is systematic single-molecule experiments, which probe the dynamics of loop formation for different DNA architectures (i.e. different sequences, different transcription factor binding strengths, different distances between transcription factor binding sites) to complement systematic *in vivo* experiments that explore these same parameters. In this paper,

we have described an example of such a systematic series of measurements, which begins to examine how the formation of transcription factor-DNA complexes depend upon parameters such as transcription factor concentration and the length of the DNA implicated in the complex.

In the case of the *lac* operon, our *in vitro* measurements demonstrate that the formation of the repressor-DNA complex does not require any helper proteins, nor does it call for supercoiling of the DNA (as appears to be required in other bacterial regulatory architectures [5, 6]). Further, we find that even in the absence of these mechanisms, which can only enhance the probability of loop formation, the formation of DNA loops by Lac repressor occurs more easily than would be expected on the basis of traditional views of DNA elasticity. A summary of the various measurements of short-length DNA cyclization and looping is shown in fig. 11. The idea of this figure is to present the diversity of data that weighs in on the subject of short length DNA elasticity. In particular, several sets of controversial measurements on DNA cyclization present different conclusions on the ease of this process at lengths of roughly 100 bp. TPM experiments like those presented here offer another avenue to resolve this issue, one that does not involve the complex ligase enzyme, the need to ensure a specific kinetic regime, nor other subtleties of the ligation reaction inherent in cyclization measurements. However, as seen in the figure, even here there are unexplained discrepancies between different TPM experiments which call for continued investigation.

Several intriguing mysteries remain which demand both further experimentation as well as theoretical analysis, e.g.: i) why are the probabilities of DNA loop formation systematically higher than would be expected on the basis of traditional arguments about DNA elasticity, and ii) what is the significance of three repressor binding sites in the wild-type *lac* operon? To explore these questions, TPM experiments with different DNA sequences between the two operators, as well as with Lac repressor mutants that are less flexible, would go a long way towards clarifying the mechanisms at work and would provide a basis for examining the even richer action at a distance revealed in the eukaryotic setting.

## 4 Materials and Methods

### 4.1 Plasmid DNAs

Plasmid DNAs, bearing two Lac repressor binding sites spaced at a designed distance, are created using a point mutation method (QuikChange site-directed mutagenesis, Stratagene) on plasmid pUC19. Plasmid pUC19 was chosen as a starting template because it is not only a high copy plasmid but also contains two Lac repressor binding sites: *O*1 and *O*3. The procedure for creating two binding sites separated by the desired distance from

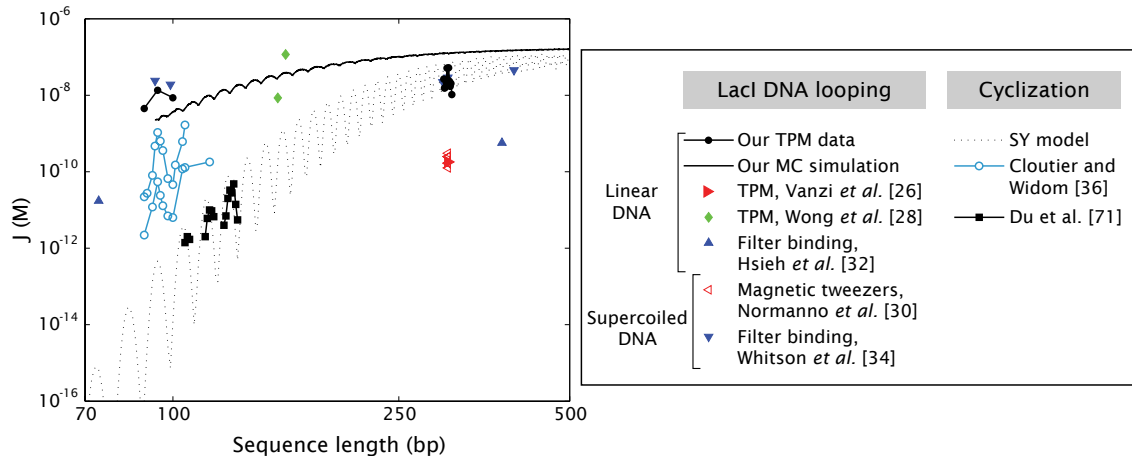


Figure 11: Effective  $J$ -factor from different experiments. Although the  $J$  factor obtained from cyclization experiments is not directly comparable to the looping  $J$  factor studied in this paper (due to the differences in geometry), we present the two quantities together as functions of loop length to summarize the work from many groups'. Error bars have been omitted for clarity. The filter binding data is an order of magnitude estimate.

template pUC19 is illustrated in fig. 12 (a). We first mutate six basepairs in the  $O3$  site converting it to  $O3^*$  in a way that eliminates the binding affinity for this site [90]. The resulting plasmid is called pUC19O1 indicating it only has a single  $O1$  site. To construct another binding site on the pUC19O1 plasmid, we replace 20bp with the Lac repressor binding sequence  $Oid$  at a series of locations differing by 1bp increments in their distance from  $O1$  using the mutagenesis method again. For some of the secondary site construction, we have to use either deletion or addition from already made plasmids with two designed binding sites. The details on primers and templates used in this process are listed in Table 2. The final product contains two binding sites  $O1$  and  $Oid$  spaced at the desired distance.

The short loop DNA (89, 94 and 100 bp) was constructed in the following way. Plasmid pZS22-YFP was kindly provided by Michael Elowitz. The main features of the pZ plasmids are located between unique restriction sites [91]. The YFP gene comes from plasmid pDH5 (University of Washington Yeast Resource Center [92]).

A variant of the lacUV5 promoter [12] was synthesized and placed between the EcoRI and XhoI sites of pZS22-YFP in order to create pZS25'-YFP. This promoter included the -35 and -10 regions of the lacUV5 promoter, an AseI site between the two signals and a  $O1$  operator at position -45 from the transcription start as shown in fig. 13(A).

The random sequence E8-89 [3, 36] was obtained by PCR from a plasmid kindly pro-



vided by Jonathan Widom. The primers used had a flanking AatII site and *Oid* operator upstream and a flanking *O1* operator, -35 region and AseI site downstream. This PCR product was combined with the appropriate digest of pZS25'-YFP to give rise to pZS25'*Oid*-E89-*O1*<sub>-45</sub>-YFP. This is shown schematically in fig. 13(B). Finally, the different lengths used by Cloutier and Widom were generated from this template using site directed mutagenesis.

## 4.2 Construction of labeled DNAs

In TPM experiments, DNA is linked between the substrate and a bead. Two pairs of linkers: biotin-streptavidin and digoxigenin-anti-digoxigenin, are chosen to permit specific linkage of the DNA to a polystyrene microsphere and glass coverslip, respectively. As illustrated in fig. 12(B), PCR was used to amplify such labeled DNA with two modified primers. Each primer is designed to be about 20 bp in length and linked with either biotin or digoxigenin at the 5' end (Eurofins MWG Operon). In the case of the long sequence constructs, in order to optimize the PCR reaction linearized plasmids with an AatII cut are used as the template. Detailed information concerning the design of our PCR reactions is listed in Table 4.3 and the constructs are shown schematically in fig. 14. The PCR products were then purified by gel extraction (QIAquick Gel Extraction Kit, QIAGEN) and the concentration of the DNA was measured using quantitative DNA electrophoresis.

## 4.3 TPM sample preparation

TPM sample preparation involves assembly of the relevant DNA tethers and their associated reporter beads. Streptavidin coated microspheres (Bangs lab) of diameter 490 nm served as our tethered particle. Prior to each usage, a buffer exchange on the beads was performed by three cycles of centrifugation and resuspension in TPB buffer (20 mM Tris-acetate, pH=8.0, 130 mM KCl, 4 mM MgCl<sub>2</sub>, 0.1 mM DTT, 0.1 mM EDTA, 20  $\mu$ g/ml acetylated BSA (Sigma-Aldrich), 80  $\mu$ g/ml heparin(Sigma-Aldrich) and 0.3% biotin-free casein colloidal buffer (RDI, Flanders, NJ)). This combination of reagents was chosen in an attempt to maximize sample yield and longevity, while minimizing non-specific adsorption of DNA and microspheres onto the coverslip.

Tethered particle samples were created inside a 20-40  $\mu$ l flow cell made out of a glass slide with one hole near each end, glass coverslip, double-sided tape and tygon tubing. The coverslip and glass slide were cleaned with plasma cleaning for 4 minutes and then the flow cell was constructed as shown in fig. 15(A). Two tygon tubes serving as an input and output were inserted into the holes on the glass slide and sealed with epoxy. A reaction chamber was created by cutting a channel on the double sided tape, which glues the coverslip and

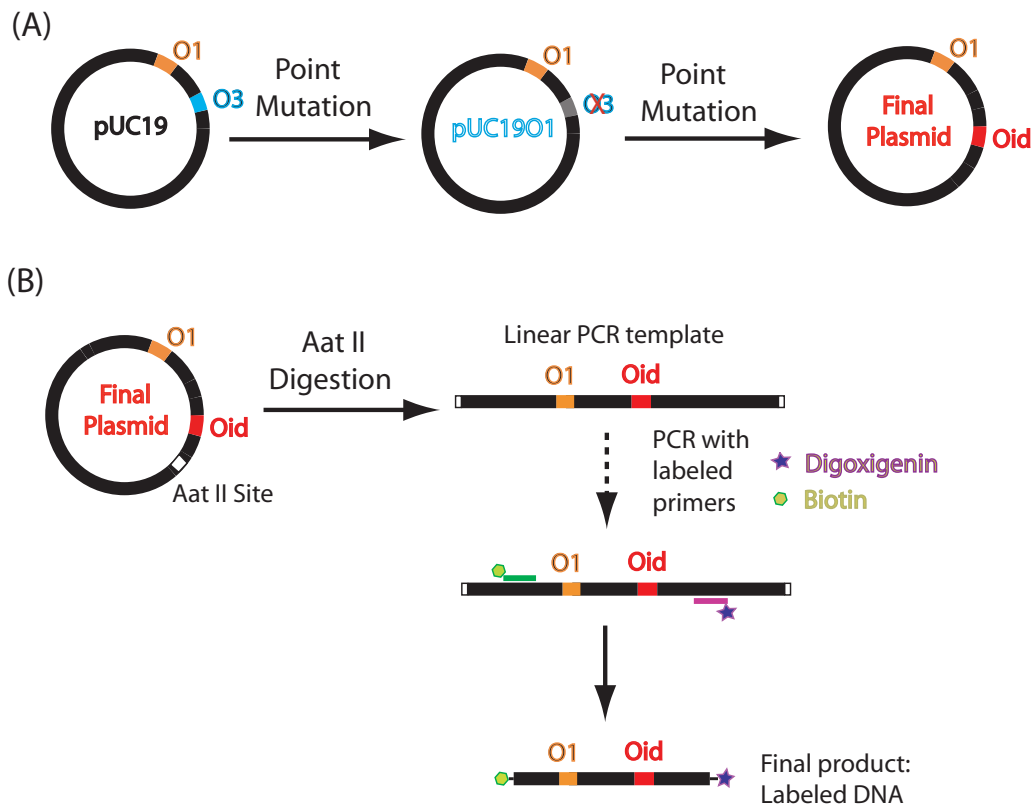


Figure 12: Synthesis of DNA construct. (A) Schematic of the procedure for construction of the plasmid with two Lac repressor binding sites. (B) Schematic of the protocol for producing labeled DNA using a PCR reaction with labeled primers.

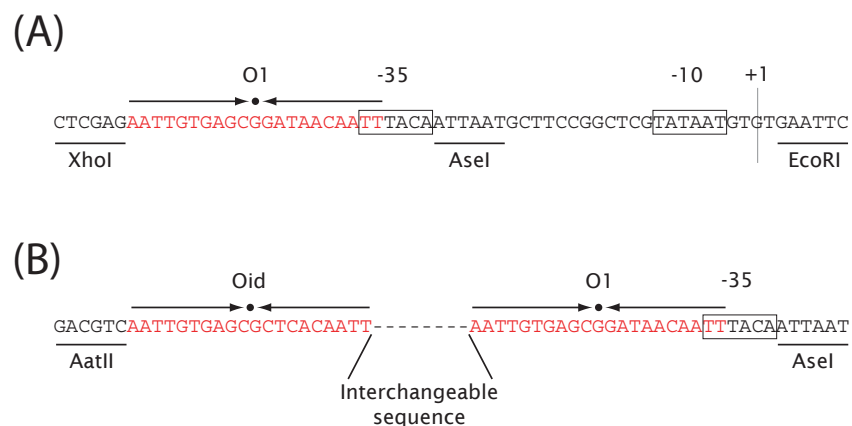


Figure 13: Promoter regions of the different short loop constructs. (A) Promoter region of pZS25-YFP which has a variant of the lacUV5 promoter and an *O1* operator upstream overlapping the -35 region. (B) Final construct that allows to insert arbitrary DNA sequences between a *Oid* and *O1* operators.

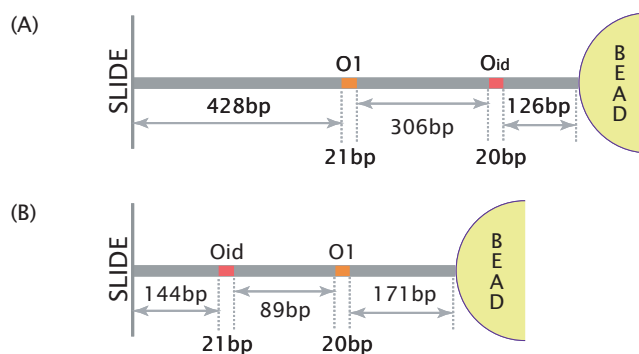


Figure 14: Examples of the tether constructs used. (A) In the long distance constructs *Oid* was displaced keeping the total construct length constant. (B) In the short distance constructs the sequence between the operators was altered, which results in each construct having a slightly different total length. (Drawings not to scale.)

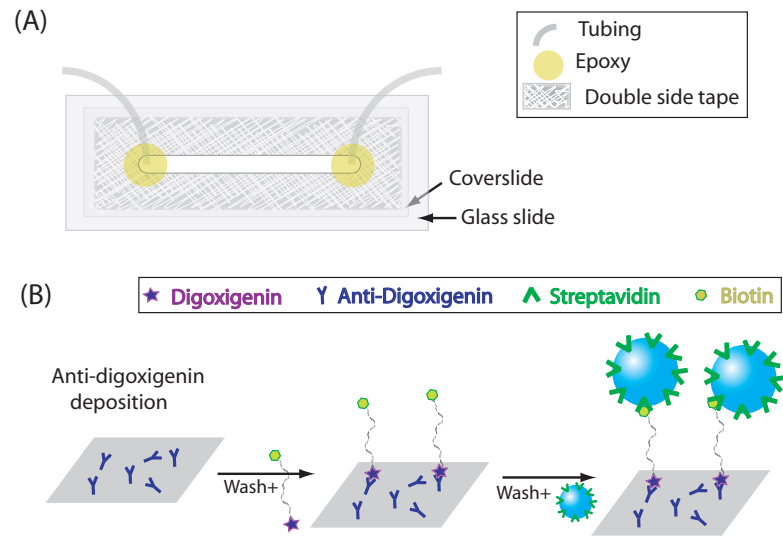


Figure 15: Illustration of TPM sample preparation. (A) Sketch of the flow cell. (B) The scheme for making DNA tethers.

glass slide together. Making the end of the channel round and as close to the holes of the glass slide as possible is important to avoid generating bubbles. The flow cell was then heated for about 20 seconds to seal securely.

For DNA tether assembly, the flow chamber was first incubated with 20  $\mu\text{g}/\text{mg}$  polyclonal anti-digoxigenin (Roche) in PBS buffer for about 25 minutes, and then rinsed with 400  $\mu\text{l}$  wash buffer (TPB buffer with no casein) followed by 400  $\mu\text{l}$  of TPB buffer. 250  $\mu\text{l}$  of labeled DNA in TPB buffer with about 2 pM concentration was flushed into the chamber and incubated for around 1 hour. Then 10 pM of beads was introduced into the chamber and incubated for 20 minutes after washing with 750  $\mu\text{l}$  TPB buffer to remove the unbound DNAs. Finally, unbound microspheres were removed by flushing the chamber with 1 mL TPB buffer. For looping experiments, 0.5 mL~1mL LRB buffer (10 mM Tris-HCl, pH 7.4, 200 mM KCl, 0.1 mM EDTA, 0.2 mM DTT, 5% DMSO and 0.3% biotin-free casein colloidal buffer (RDI, Flanders, NJ)) containing the desired concentration of Lac repressor (a kind gift from Kathleen Matthews' lab) was then flushed into the chamber and incubated about 15 minutes before observation.

#### 4.4 Data Acquisition and Processing

The motion of the bead is recorded through a Differential Interference Contrast (DIC) microscope at 30 frames per second. The position of the bead is tracked in the x-y plane using a cross-correlation method [94] and recorded as raw data for further analysis. Such raw positional data are subject to a slow drift due to vibrations of the experimental apparatus. A drift correction is then applied using a high pass first-order Butterworth filter at cutoff frequency 0.1Hz [26]. From the filtered data,  $R^2(t)$  is then calculated as  $x(t)^2 + y(t)^2$  and a running average  $\sqrt{\langle R^2(t) \rangle}$  is obtained using a Gaussian filter at cutoff frequency 0.033 Hz [26, 95], which corresponds to the standard deviations of the filter's impulse response time of 4 s. The traces shown in this paper are all obtained in this way.

**Acknowledgements** We are extremely grateful to a number of people who have been generous with their ideas, time and materials. Jon Widom has given us help of all kinds since we first began down the path of trying to make these measurements. Jeff Gelles has continuously helped us along with insights from the very beginning when one of us (RP) didn't even know what DIC microscopy was. Similarly, Laura Finzi and David Dunlap were kind enough to host one of us (LH) in their lab and to provide constant encouragement, advice and insights. Bob Schleif has patiently advised us on many aspects of this project and has served as a looping sage for many years. Kathleen Matthews and Jason Kahn have both been extremely generous with both ideas and in providing us protein. We also thank Sankar Adhya, David Bensimon, Nily Dan, Paul Grayson, Heun Jin Lee, John Maddocks,

Molecule	Primer	Template	Action	Resulting Molecule
pUC19O1	Mut0	pUC19	Replace	O1
pUC300	Mut1	pUC301	Delete 1bp	O1-300bp-Oid
pUC301	Mut2	pUC19O1	Replace	O1-301bp-Oid
pUC302	Mut3	pUC19O1	Replace	O1-302bp-Oid
pUC303	Mut4	pUC19O1	Replace	O1-303bp-Oid
pUC304	Mut5	pUC19O1	Replace	O1-304bp-Oid
pUC305	Mut6	pUC19O1	Replace	O1-305bp-Oid
pUC306	Mut7	pUC19O1	Replace	O1-306bp-Oid
pUC307	Mut8	pUC19O1	Replace	O1-307bp-Oid
pUC308	Mut9	pUC19O1	Replace	O1-308bp-Oid
pUC309	Mut10	pUC308	Add 1bp	O1-309bp-Oid
pUC310	Mut11	pUC308	Add 2bp	O1-310bp-Oid

Primer sequences(5' -> 3'):

Mut0: ctaactcacattaattgcgttgAgctcGAGgTTcgctttccagtc

Mut1: catacgagccggaag (G) cataaagtgtaaagc

Mut2: ctcgaaagaaca AATTGTGAGCGCTCACAATT aaggccaggaacc

Mut3: ctcgaaagaacat AATTGTGAGCGCTCACAATT aggccaggaaccg

Mut4: cggaaagaacatg AATTGTGAGCGCTCACAATT gccaggaaccgt

Mut5: ggaaagaacatgt AATTGTGAGCGCTCACAATT gccaggaaccgta

Mut6: gaaagaacatgtg AATTGTGAGCGCTCACAATT ccaggaaccgtaa

Mut7: cggaaagaacatgtga AATTGTGAGCGCTCACAATT caggaaccgtaaaaag

Mut8: ggaaagaacatgtgag AATTGTGAGCGCTCACAATT aggaaccgtaaaaagg

Mut9: gaaagaacatgtgagc AATTGTGAGCGCTCACAATT ggaaccgtaaaaaggc

Mut10: catacgagccggaag [C] cataaagtgtaaagc

Mut11: catacgagccggaag [CG] cataaagtgtaaagc

Table 2: Materials used in the mutagenesis process for creating plasmids with two Lac repressor binding sites. The capital letters in the primer sequences indicate the mutations. '()' indicates bp deletion and '[' ]' indicates bp addition. The inter-operator distance indicated here is the distance between two inner edges of the operators instead of center to center distance that is commonly used in *in vivo* experiments [13, 14, 15, 90, 93].

Molecule	Template	Length(bp)	Resulting
pUC300L1	pUC300	900	Dig - 427bp-O1-300bp-Oid-132bp - Bio
pUC301L1	pUC301	901	Dig - 427bp-O1-301bp-Oid-132bp - Bio
pUC302L1	pUC302	901	Dig - 427bp-O1-302bp-Oid-131bp - Bio
pUC303L1	pUC303	901	Dig - 427bp-O1-303bp-Oid-130bp - Bio
pUC304L1	pUC304	901	Dig - 427bp-O1-304bp-Oid-129bp - Bio
pUC305L1	pUC305	901	Dig - 427bp-O1-305bp-Oid-128bp - Bio
pUC306L1	pUC306	901	Dig - 427bp-O1-306bp-Oid-127bp - Bio
pUC307L1	pUC307	901	Dig - 427bp-O1-307bp-Oid-126bp - Bio
pUC308L1	pUC308	901	Dig - 427bp-O1-308bp-Oid-125bp - Bio
pUC309L1	pUC309	902	Dig - 427bp-O1-309bp-Oid-125bp - Bio
pUC310L1	pUC310	903	Dig - 427bp-O1-310bp-Oid-125bp - Bio
E8-89	pZS25' <i>Oid</i> -E89-O1 <sub>-45</sub> -YFP	445	Dig - 144bp-Oid-89bp-O1-171bp - Bio
E8-94	pZS25' <i>Oid</i> -E94-O1 <sub>-45</sub> -YFP	450	Dig - 144bp-Oid-94bp-O1-171bp - Bio
E8-100	pZS25' <i>Oid</i> -E100-O1 <sub>-45</sub> -YFP	456	Dig - 144bp-Oid-100bp-O1-171bp - Bio

Primer sequences(5' -> 3'):

Plen901F: Dig - ACAGCTTGTCTGTAAGCGGATG

Plen901R: Bio - CGCCTGGTATCTTTATAGTCCTGTC

PF1: Dig - ATGCGAAACGATCCTCATCC

PR1: Bio - GCATCACCTTCACCCTCTCC

Table 3: Materials used in amplifying labeled DNA using PCR. The inter-operator distances indicated here is the distance between two inner sides of the operators instead of center to center distance. Primers Plen901F and Plen901R were used for the long distance constructs. Primers PF1 and PR1 were used for the short distance constructs.

Keir Neuman, Tom Perkins, Steve Quake, Andy Spakowitz, Terence Strick, Paul Wiggins, Jie Yan, and Sylvain Zorman for many discussions. RP and LH acknowledge the support of the Keck Foundation, National Science Foundation grant Nos. CMS-0301657 and CMS-0404031, and the National Institutes of Health Directors Pioneer Award grant No. DP1 OD000217. HG is grateful for support from both the NSF funded NIRT and the NIH Directors Pioneer Award. PCN, KBT, and JFB were partially supported by NSF grants DGE- 0221664, DMR04-25780, and DMR-0404674.



## 5 Supplementary Materials

### 5.1 Bead Selection, Data Rejection and “Representative Data”

One of the most important challenges of these experiments (and perhaps any single-molecule experiment based upon watching the motions of beads tethered to single molecules) is devising systematic methods for deciding which beads are “qualified” and how to reject trajectories that are anomalous without biasing the results [19, 20, 21, 78]. To that end, we have attempted to institute a number of criteria for performing data selection that are indicated schematically in figs. 16 and 17. The first attempt to “objectively” select qualified beads takes place by excising segments of the traces corresponding to the unlooped state and examining whether their motions are symmetric (i.e. jiggle in the x- and y-directions in the same way) as evidenced by the probability distribution for the x- and y-excursions. This screening permits us to select beads within a given field of view that are ostensibly properly tethered. Examples of these selection criteria are shown in fig. 16 for the particular case where no protein is present. Typically, a fraction of roughly 20 ~ 30 % of the beads are rejected as a result of failure to exhibit proper symmetry or because they are stuck.

A more tricky question arises when we have to assess whether something went wrong during data acquisition that requires either all or part of a given TPM trajectory to be rejected. In some cases, the offending behavior is evident at the level of the bare images of the jiggling beads. For example, a given bead can become stuck to the surface or the DNA can break and the bead will disappear from the field of view. These events have a signature of spikes in the  $R_{\text{RMS}}$  traces as shown in fig. 17. A movie corresponding to the event shown in fig. 17(A) can be found as a Supplementary Movie.

Fig. 17 also shows an example of data that was kept with an offending region highlighted that was removed. Note that if the spike regions in trajectories were actually kept, it would have no bearing on histograms like those shown in figs. 2 and 6 since the spikes will show up as features on the tails of the histograms. On the other hand, by excising certain pieces of trajectories, there can be some effect on the kinetic claims we would be able to make since these anomalies will cause errors in the dwell time measurements.

In none of the cases considered in this work were sticking events observed in any significant number. Assuming that sticking is mainly due to nonspecific interactions with the bead and the surface one would expect the shorter constructs to show the most sticking events. In order to control for this we performed TPM experiments using tethers of 351 bp in length in the absence of Lac repressor. This length is comparable to the length the short constructs (E889, E894 and E8100) would have if the sequence between the *lac* operators was removed. Out of 18 tethers characterized only 5 showed any sticking events. In those

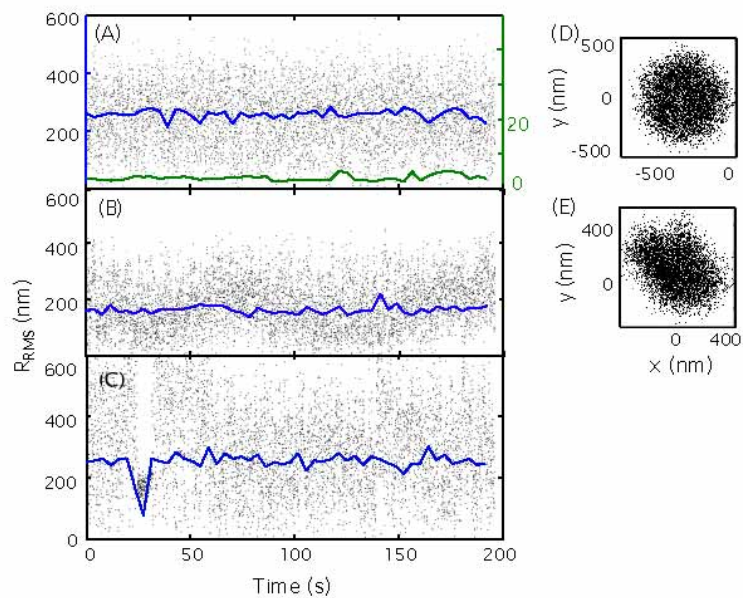


Figure 16: Conceptual description of data selection. All traces in this case are taken in the absence of Lac repressor and are used as the basis of choosing qualified beads for the looping study. (A) Experimental traces for a bead exercising symmetric motion (blue) and for a stuck bead (green). (B) Trajectory for a bead that exhibits non symmetric motion. (C) Trajectory for a bead that exhibits a transient sticking event. (D) Positional data for a bead that exhibits symmetric motion. (E) Positional data corresponding to the trajectory shown in (B) and for which the motion is not symmetric.

5 traces, the sticking events corresponded to less than 4 % of the observation time for each bead (data not shown). In order to discard any contribution to the sticking events from the presence of the protein, Lac repressor was flowed in the presence of 1 mM IPTG which serves to eliminate the binding of Lac repressor to the DNA (or at least drastically reduce it). The goal of this control is to see whether the presence of unbound protein somehow induces unwanted sticking events. Out of the 7 tethers characterized all showed sticking events, but these corresponded to less than 1 % of the time. Finally, there is still the chance that Lac repressor that is specifically bound to the tether might contribute to sticking. In order to test this hypothesis we used a construct of this length with only one binding site. Here too (data not shown), there was no significant sticking lending further support for the idea that even for the short tethers, we are able to detect looping.

In order to produce histograms like those shown in figs. 2 and 6 we have to sum over the histograms resulting from many individual trajectories. Fig. 1 shows the connection between an individual TPM trace for a single bead and its corresponding motion histogram. However, since each trajectory has its own unique features, it is of interest to see how the smoothed histogram resulting from many individual trajectories emerges from the averaging process. Fig. 18 shows the motion histogram obtained by averaging over the histograms from progressively larger numbers of individual trajectories.

Now that we have seen some of the pitfalls associated with TPM trajectories, we show “representative” examples of the individual trajectories culminating in figs. 2 and 6. Fig. 19 shows multiple examples of trajectories resulting from different concentrations of Lac repressor. Even at the level of visual inspection of these individual trajectories, it is evident that there are two distinct looping states and that the relative occupancies of the different looped and unlooped states depend upon the concentration of repressor. Similar results are shown in figs. 20 and 21 which illustrates multiple individual trajectories for the case in which the interoperator spacing (rather than the Lac repressor) concentration is the experimental dial that we tune to vary the looping stability.

## 5.2 Data Analysis and Probabilities Calculation

The data shown in figs. 2 and 6 characterizes the results of many different TPM trajectories for each condition (Lac repressor concentration or interoperator spacing). We are interested in obtaining the probabilities associated with each state and to that end, we have tried a variety of different approaches to examine the sensitivity of the results to method of data analysis.

The first analysis we explored is based on directly looking at histograms such as those shown in figs. 2 and 6. As mentioned in the main text, these histograms are the result of

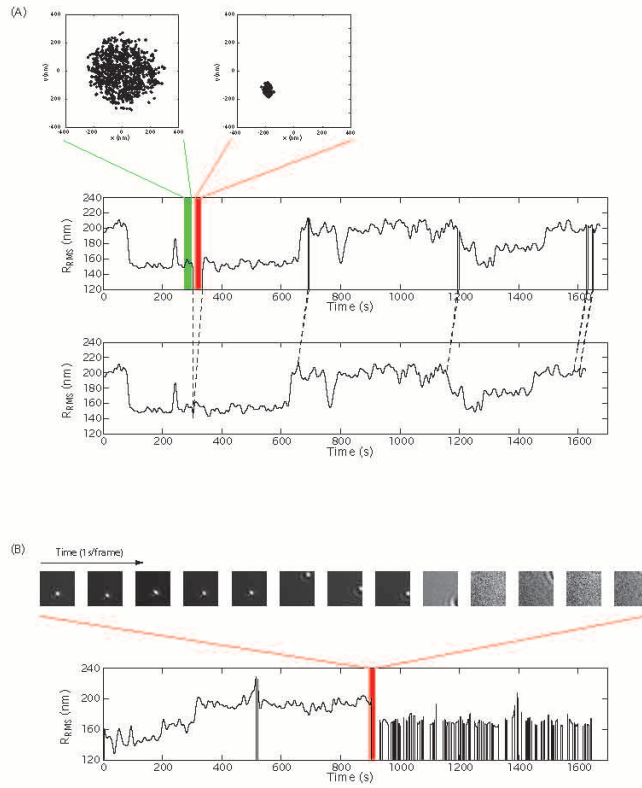


Figure 17: Transient sticking events and tether breaking. (A) A transient sticking event is revealed by a dramatic reduction in the movement of the bead and is associated with a spike in the  $R_{RMS}$  trace. These “offending” regions of the traces can be excised out which will not affect the resulting histogram, but might present an issue for any kinetic analysis as discussed in the text. A movie corresponding to this event is provided as a Supplementary Movie. (B) Signature of a tether breaking.

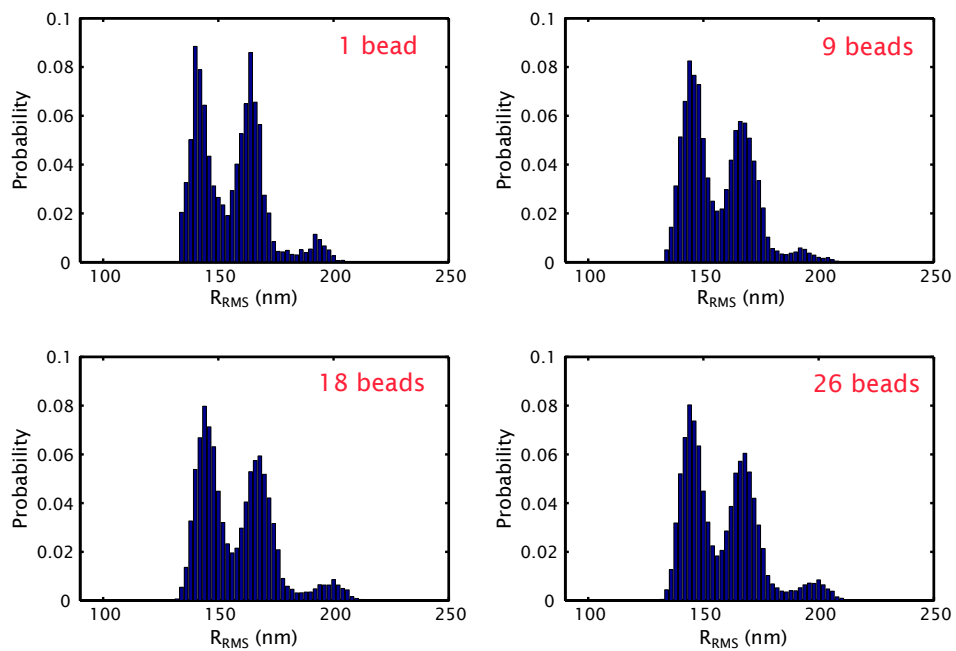


Figure 18: Effect of averaging on the data. These four histograms show the effects of including different numbers of beads in determining the overall average. Data obtained with pUC306L1 DNA in the presence of 10 pM Lac repressor.

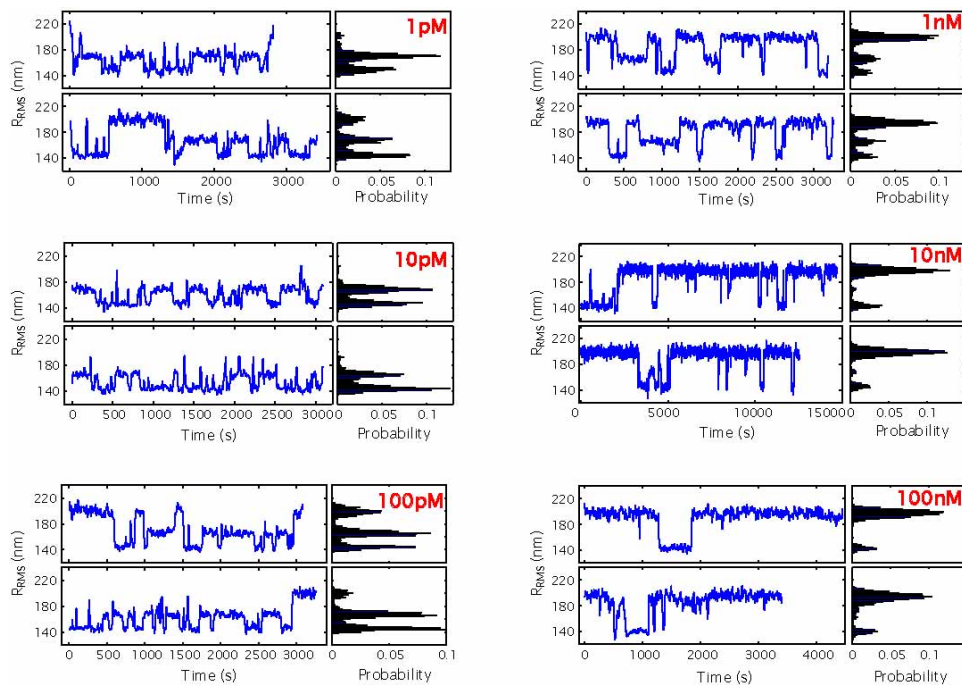


Figure 19: Concentration dependence of TPM trajectories. Representative examples of TPM trajectories. Typical TPM trajectories of the DNA tethered beads in the presence of different concentrations of Lac repressor varying from 1 pM to 100 nM. The total DNA length is 901 bp and the interoperator spacing is 306 bp.

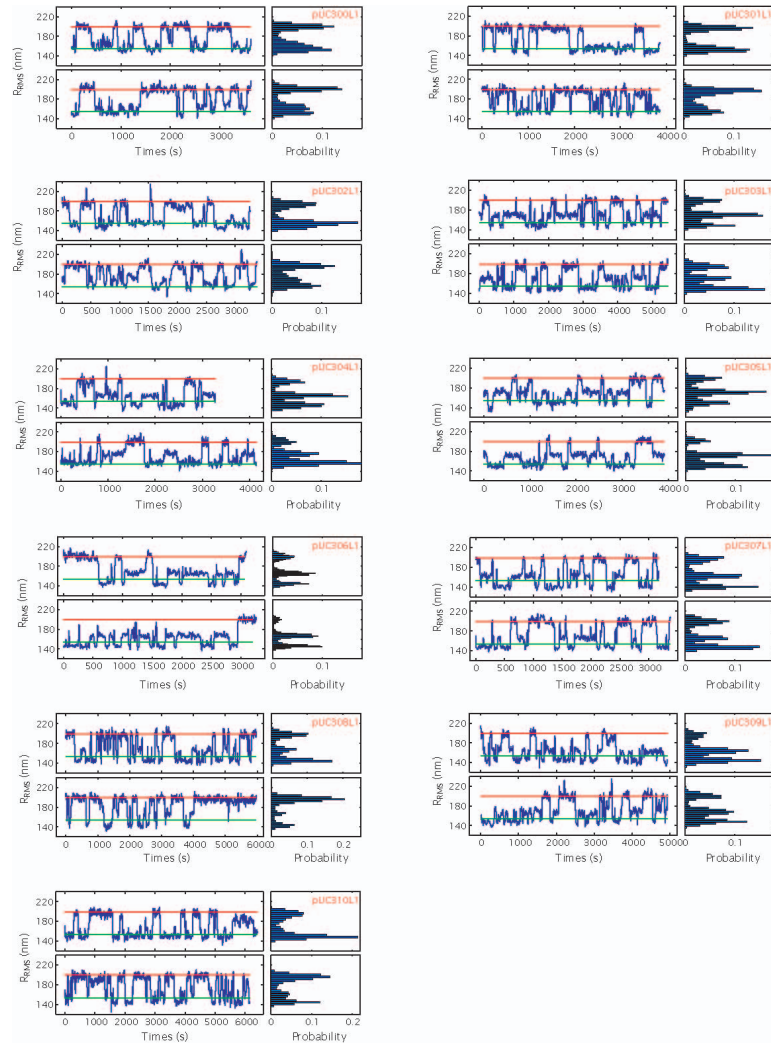


Figure 20: Length dependence of TPM trajectories. Typical TPM trajectories of the DNA tethered beads with interoperator spacing from 300 to 310 bp in 1 bp increments. The concentration of Lac repressor used in this set of experiments was 100 pM. The distance between the two operators is indicated in the naming of the construct.

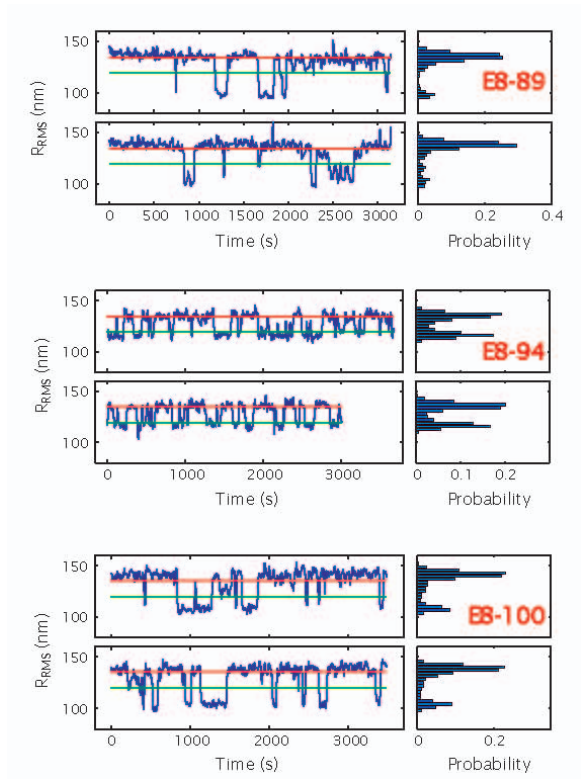


Figure 21: Typical TPM trajectories for DNA tethered beads with interoperator spacing of 89 bp, 94 bp and 100 bp. E8 refers to the particular sequence used in these experiments. The concentration of Lac repressor used to generate these trajectories is 100pM. The red and green lines indicate the expected excursion for the unlooped and looped states, respectively, where the expected length of the looped state is based upon subtracting the interoperator spacing from the overall tether length.



adding up the normalized contribution from each bead. One scheme for carrying this out is to fit the histogram to the sum of three Gaussians. The idea of such a fit is that there is a main peak associated with the unlooped state and then two separate looping peaks, each of which is fit with its own Gaussian. With the fitting results in hand the area under each Gaussian can be computed, which leads to a probability assignment. We call this scheme “Gaussian Integral”.

An alternative scheme is to define thresholds between the different states. The bins on either side of the thresholds are then added, giving the different probabilities. We explore two ways of calculating the thresholds: i) Finding the minimum between adjacent Gaussians from the fit described previously (“Gaussian Minimum”), and ii) finding the minimum in the histograms between peaks (“Histogram Minimum”).

Finally, we have also explored the use of alternatives such as the Diffusive Hidden Markov Model (“dHMM”). The Diffusive Hidden Markov Model (DHMM) method is applied to do the kinetic analysis [96, 97] and for our present purposes permits us a different way to determine the looping probability by telling us the fraction of time spent in each of the distinct states. This method employs the concept of HMM and customizes it in a way suitable for TPM data, through which the rate constants are directly derived from the positional data obtained in the TPM experiments. To characterize the dynamical information of the beads in each state, control experiments are performed in the following ways: i) To obtain the information for the unlooped state, the bead’s motion is observed in the absence of the DNA looping protein Lac repressor. ii) For the looped state, we monitor the bead’s motion in the presence of a Lac repressor mutant V52C instead of Lac repressor itself. This mutant is designed to permit disulfide bond formation, which makes important contacts that are critical to DNA binding. As a result, V52C has increased affinity for DNA operators [98], leading to a measurement of primarily looped states. Such data containing only one type of looped state is selected to obtain the information that serves as input to the HMM model. One of the outcomes of the HMM analysis is an explicit statement about the amount of time spent in each of the states which can be used in turn to compute the looping probability.

One argument against the previously mentioned schemes is that they do not capture the variability inherent in single molecule experiments. Each tether will behave in a slightly different way, as is illustrated in fig. 22 for construct pUC300L1. Notice that even though the two looped states were overlapping in fig. 6 they are discernable in most individual traces. Fig. 22(F) also shows a case where no call on the identity of the looped state could be made. For the long length constructs where this happened only a small fraction of the beads, between 2% and 6% would show this type of histogram. Identification of the individual loops becomes more problematic in the short length constructs. In this case

around 10% of the beads would show this behavior.

The looping probabilities obtained using all these methods are shown in fig. 23. We conclude that there is no significant variation in the results from any of the different approaches. In section 5.4 we show that the quantitative parameters extracted from these different looping probabilities do not differ significantly. Finally, figs. 24 and 25 show the looping probability for each individual state in the cases where both states were discernible. Ultimately, it would be of great interest to use experiments like those described here to determine the looping free energies (or  $J_{loop}$ s for the different states. This is presented in section 5.5.

### 5.3 Theoretical Analysis of Looping

Statistical mechanics provides a powerful tool for dissecting the DNA-protein interactions that take place during transcriptional regulation. We find it convenient to derive the various expressions for binding probabilities using simple lattice models of DNA binding proteins and their DNA targets. These models can then be reinterpreted in the familiar language of equilibrium constants and effective  $J$ -factors. In this section, we sketch the derivations of the formulae used in the main body of the paper. An alternative derivation appears in [41].

#### 5.3.1 Simple binding of Lac repressor

In a lattice model, we imagine the solution as discretized into a set of  $\Omega$  boxes of volume  $v$ . The  $R$  repressors are free to occupy any of these distinct boxes which provide a simple and convenient basis for computing the entropic contribution to the overall free energy. A repressor in solution has an energy  $\varepsilon_{sol}$  which appears in the Boltzmann factor. The configurational degrees of freedom (both translational and rotational) in this model are taken care of by assigning the molecules to one of the  $\Omega$  boxes available in our lattice model of the solution and by noting that there is a factor of  $\frac{8\pi^2}{\delta\omega}$  associated with its rotational degrees of freedom ( $4\pi$  for the directions in which the molecule can point on the unit sphere and  $2\pi$  for the rotation around the protein’s axis). The partition function of  $R$  repressors in the solution is

$$Z_{sol} = \binom{\Omega}{R} e^{-\beta R \varepsilon_{sol}} \left( \frac{8\pi^2}{\delta\omega} \right)^R . \quad (7)$$

Now we introduce a DNA molecule with one binding site. This case is appropriate when LacI is in excess of the DNA. When one Lac repressor from the solution binds to the operator it now has an energy  $\varepsilon_b$  associated with the binding itself and a “tether” energy  $\varepsilon_t$  associated with the extra head that is still in the solution. Next, we exploit the fact that

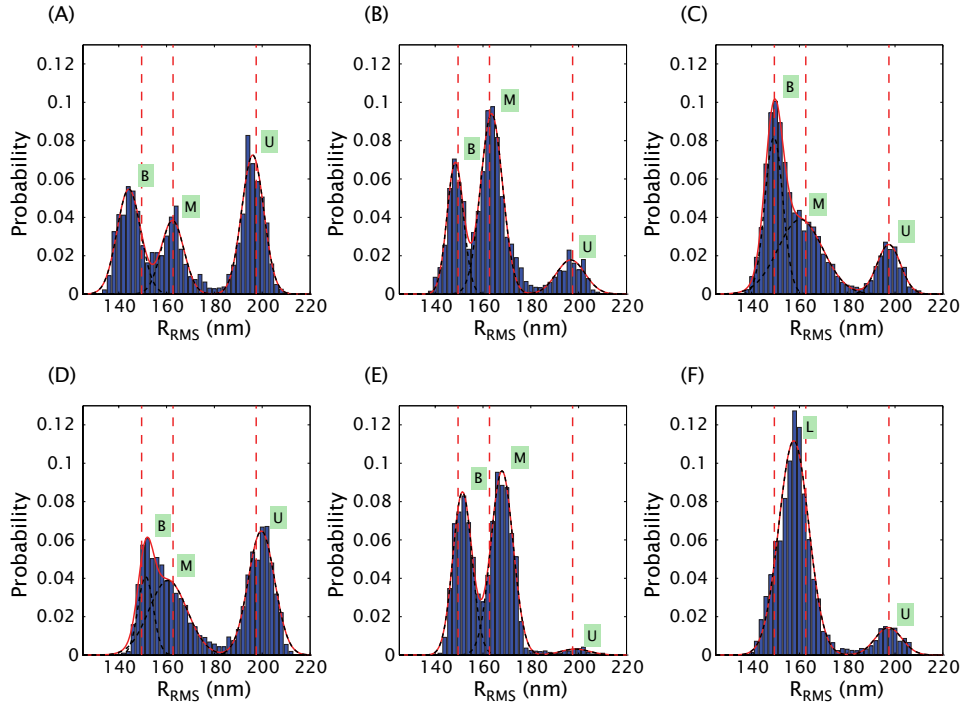


Figure 22: Rogues gallery of individual bead histograms. Three Gaussian fit to individual bead traces corresponding to the pUC300L1 construct. The vertical dashed lines correspond to the locations of the peaks as revealed by a three Gaussian fit to the corresponding histogram of fig. 6. The black dashed line are the individual Gaussians, while the solid red line is their sum. (A-E) The peaks are labeled B (bottom loop), M (middle loop), and U (unlooped state). In the small fraction of cases that no decision about the identity of the looped state could not be discerned the label L (looped state) is used.

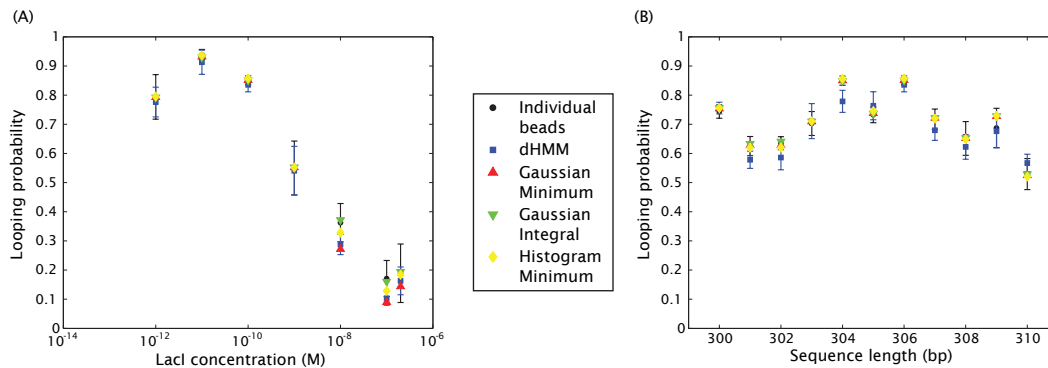


Figure 23: Different approaches for calculating the looping probability. The looping probability as a function of (A) concentration and (B) sequence length, calculated using the approaches described in the text.

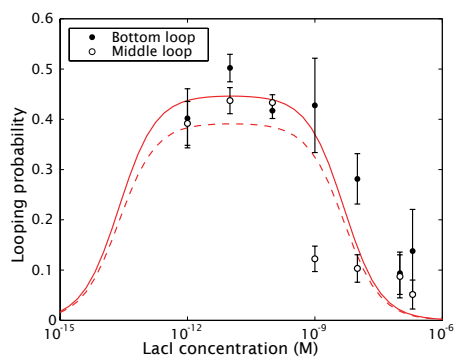


Figure 24: Individual loops vs. concentration. Probability of each looped state as a function of concentration. The lines are fits to the nonlinear model from eqn. 22.

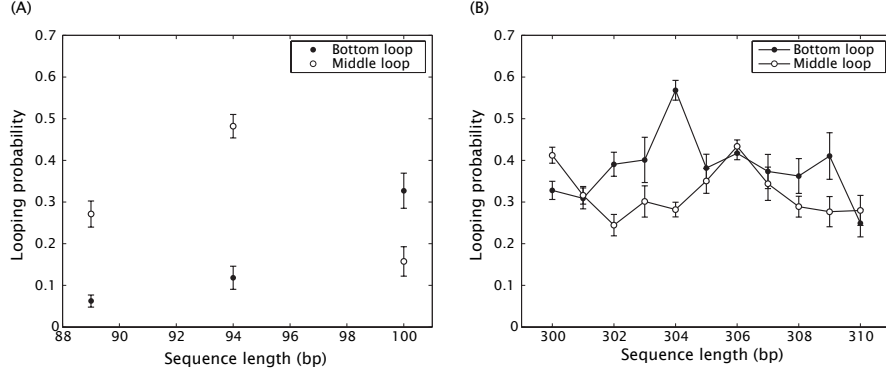


Figure 25: Individual loops vs. phasing. Probability of each looped state as a function of sequence length. (A) Short loops, (B) a full cycle at 300 bp.

we can choose either head to bind to the operator of interest and this head can bind in two distinct orientations, yielding a factor of 4 degeneracy in this state. The total partition function is

$$Z = Z_{sol}(R) + 4Z_{sol}(R - 1)e^{-\beta(\varepsilon_b + \varepsilon_t)}. \quad (8)$$

This translates into the following probability of binding

$$p_{bound} = \frac{4 \frac{\delta\omega}{8\pi^2} \frac{R}{\Omega} e^{-\beta\Delta\varepsilon}}{1 + 4 \frac{\delta\omega}{8\pi^2} \frac{R}{\Omega} e^{-\beta\Delta\varepsilon}}, \quad (9)$$

where we have defined  $\Delta\varepsilon = \varepsilon_b + \varepsilon_t - \varepsilon_{sol}$ .

We recover the usual formula when characterizing binding using dissociation constants

$$p_{bound} = \frac{[R]/K_d}{1 + [R]/K_d}, \quad (10)$$

if we make the identification

$$K_d = \frac{1}{4v} \frac{8\pi^2}{\delta\omega} e^{\beta\Delta\varepsilon}. \quad (11)$$

With this result in hand we are ready to address the more complex case of DNA looping.

### 5.3.2 DNA looping by Lac repressor

We now have two operators, each one with a binding energy  $\varepsilon_1$  and  $\varepsilon_{id}$ , corresponding to the operators  $O1$  and  $Oid$ , respectively. We consider the usual five classes of states that

include: i) free operators, ii+iii) one of the operators occupied, iv) both operators occupied by different LacI molecules, and v) LacI looping both operators, which can happen in multiple configurations. The partition function is

$$\begin{aligned}
Z &= Z_{sol}(R) + 4Z_{sol}(R-1)e^{-\beta\varepsilon_t} \left( e^{-\beta\varepsilon_1} + e^{-\beta\varepsilon_{id}} \right) \\
&\quad + 16Z_{sol}(R-2)e^{-\beta(\varepsilon_1+\varepsilon_{id}+2\varepsilon_t)} + \\
&\quad + \sum_i Z_{sol}(R-1)e^{-\beta(\varepsilon_1+\varepsilon_{id}+F_{loop,i})}.
\end{aligned} \tag{12}$$

The factors of 4 in the second and third term correspond to the degeneracy described above. The factor of 16 in the fourth term accounts for all of the different ways of binding two repressors independently. Here we defined  $F_{loop,i}$  as the looping free energy associated with a particular configuration (orientation of operators with respect to the molecule). The sum in the last term includes all four possible loop topologies [38, 49] and the fact that we are thinking of the two binding heads of LacI as being distinguishable. Defining  $\alpha$  and  $\beta$  as state variables that describe the orientation of  $O1$  and  $Oid$  with respect to the binding heads, respectively we can write the sum as

$$\sum_i = \sum_{\text{heads}} \sum_{\alpha,\beta}. \tag{13}$$

The sum over the heads results in a factor of two, since none of the terms inside the sum actually depend on that choice. We next define the overall looping energy  $\Delta F_{loop}$  by

$$e^{-\beta\Delta F_{loop}} = \frac{1}{\sum_{\alpha,\beta} 1} \sum_{\alpha,\beta} e^{-\beta F_{loop,\alpha,\beta}} = \frac{1}{4} \sum_{\alpha,\beta} e^{-\beta\Delta F_{loop,\alpha,\beta}}. \tag{14}$$

Using the calculations and definitions from section 5.3.1 we arrive at the looping probability

$$\begin{aligned}
p_{loop} &= \left[ 8 \frac{R}{\Omega} \frac{\delta\omega}{8\pi^2} e^{-\beta(\Delta\varepsilon_1+\Delta\varepsilon_{id}+\Delta F_{loop}+2\varepsilon_t-\varepsilon_{sol})} \right] \\
&\quad \left[ 1 + 4 \frac{R}{\Omega} \frac{\delta\omega}{8\pi^2} \left( e^{-\beta\Delta\varepsilon_1} + e^{-\beta\Delta\varepsilon_{id}} \right) + 16 \frac{R(R-1)}{\Omega^2} \left( \frac{\delta\omega}{8\pi^2} \right)^2 e^{-\beta(\Delta\varepsilon_1+\Delta\varepsilon_{id})} + \right. \\
&\quad \left. 8 \frac{R}{\Omega} \frac{\delta\omega}{8\pi^2} e^{-\beta(\Delta\varepsilon_1+\Delta\varepsilon_{id}+\Delta F_{loop}+2\varepsilon_t-\varepsilon_{sol})} \right]^{-1}.
\end{aligned} \tag{15}$$

Notice that the term that corresponds to looping has the energy  $\Delta F_{loop} + 2\varepsilon_t - \varepsilon_{sol}$ . In

principle this is the parameter associated with looping, but it also includes information about the energetics of LacI when it is in solution and when it has only one head bound to the DNA. However, we can make the assumption that the energy associated with having half a LacI in solution,  $\varepsilon_t$  is half the energy of having a full LacI in solution,  $\varepsilon_{sol}$ . This is equivalent to saying that there is no change in the energetics of binding if the other head is already bound, that there is no allosteric cooperativity. If this is true then the parameter obtained from an experiment where  $p_{loop}$  is measured will actually be  $\Delta F_{loop}$ .

Since we measure concentration of Lac repressor rather than absolute number of repressor molecules we want to rewrite this formula as a function of  $[R]$  using the lattice definitions

$$\frac{R}{\Omega} = \frac{R}{\Omega v} v = [R]v. \quad (16)$$

The parameter  $v$  corresponds to the volume of a lattice site, which means that  $\Omega v$  corresponds to the whole volume. We now make the choice of a standard concentration

$$\frac{1}{v} \frac{8\pi^2}{\delta\omega} = 1 \text{ M}, \quad (17)$$

which turns the looping probability from eqn. 15 into

$$p_{loop} = \left[ 8 \frac{[R]}{1 \text{ M}} e^{-\beta(\Delta\varepsilon_1 + \Delta\varepsilon_{id} + \Delta F_{loop})} \right] \left[ 1 + 4 \frac{[R]}{1 \text{ M}} \left( e^{-\beta\Delta\varepsilon_1} + e^{-\beta\Delta\varepsilon_2} \right) + 16 \left( \frac{[R]}{1 \text{ M}} \right)^2 e^{-\beta(\Delta\varepsilon_1 + \Delta\varepsilon_{id})} + 8 \frac{[R]}{1 \text{ M}} e^{-\beta(\Delta\varepsilon_1 + \Delta\varepsilon_{id} + \Delta F_{loop})} \right]^{-1}. \quad (18)$$

Finally, we make the connection to the thermodynamic formalism using eqns. 11 and by defining that

$$J_{loop} = \frac{1}{v} \frac{8\pi^2}{\delta\omega} e^{-\beta\Delta F_{loop}}. \quad (19)$$

The point here is to use simple binding to define the parameters  $K_1$ ,  $K_{id}$  and cyclization to assign the parameter  $J_{loop}$  [99]. Here, we use a looping  $J_{loop}$  factor rather than the regular factor  $J$  factor to emphasize the fact that the boundary conditions are different from those present in cyclization, where  $J$  is clearly defined [100]. In this way, we appeal to these other experiments semantically and plug their definitions into the expression for

the looping probability derived above. This results in

$$p_{\text{loop}} = \frac{\frac{1}{2} \frac{[R]J_{\text{loop}}}{K_1 K_{id}}}{1 + \frac{[R]}{K_1} + \frac{[R]}{K_{id}} + \frac{[R]^2}{K_1 K_{id}} + \frac{1}{2} \frac{[R]J_{\text{loop}}}{K_1 K_{id}}}, \quad (20)$$

where  $J_{\text{loop}}$  is the average of the individual  $J_{\text{loop}}$  factors over  $\alpha$  and  $\beta$  as defined in eqn. 3.

In the case where we distinguish between bottom and middle looped states we can split  $J_{\text{loop}}$  into their corresponding looping  $J$  factors

$$J_{\text{loop}} = \frac{1}{2} (J_{\text{loop,B}} + J_{\text{loop,M}}). \quad (21)$$

In this case, for example, the probability of looping into the bottom state can be written as

$$p_{\text{loop}} = \frac{\frac{1}{4} \frac{[R]J_{\text{loop,B}}}{K_1 K_{id}}}{1 + \frac{[R]}{K_1} + \frac{[R]}{K_{id}} + \frac{[R]^2}{K_1 K_2} + \frac{1}{2} \frac{[R]J_{\text{loop}}}{K_1 K_{id}}}. \quad (22)$$

## 5.4 Comparison of Theory and Experiment

One of the important goals of this work is to demand a rich interplay between theories of transcriptional regulation and corresponding experiments. To that end, the entirety of the data presented in the paper is viewed through the prism of the statistical mechanics model described above.

One of the questions that we have examined is how the statistical mechanics fit depends upon the choice of how we analyze the data to determine the looping probability. Examples of different schemes for determining the looping probability and their allied fits are shown in fig. 26. In the main body of the paper, we presented looping probabilities based upon Gaussian fits to the looping peaks. However, we have also explored the use of alternatives such as the Diffusive Hidden Markov Model.

Another point of curiosity concerns the extent to which our fits for the equilibrium constants and effective  $J$ -factor depends upon which points from fig. 3 are actually used to make the fit. Fig. 27 shows the fit to both  $K_1$  and  $J_{\text{loop}}$  as a function of the particular model (nonlinear or linear) and range of data points from fig. 3 that are used in the fit. The key observation is that the final two data points (i.e. those at the largest concentrations of Lac repressor) lead to a systematic shift in the values for both  $K_1$  and  $J_{\text{loop}}$  when fitting using the linear model from eqn. 4. Another interesting point revealed by fig. 27(A) is that the full nonlinear model fit results in a value for  $K_1$  that is too large relative to the literature value by roughly a factor of 10, corresponding to a difference in binding energy



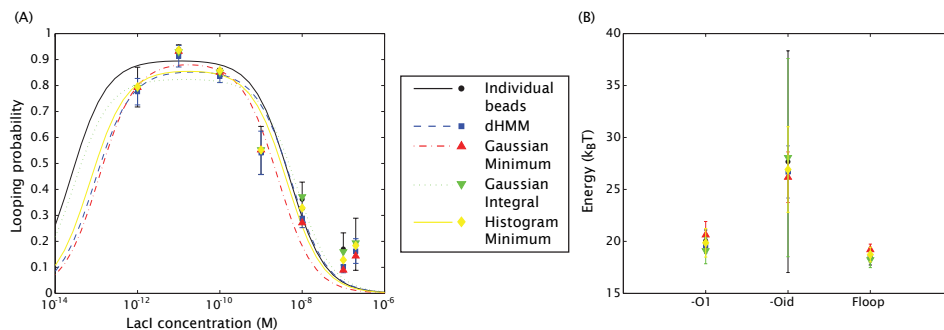


Figure 26: Alternative methods for fitting the looping probabilities. (A) Different schemes for determining the looping probability from the data result in slightly different fits for the concentration dependent data. (B) Results of the various fits performed in (A). Notice how the model cannot constrain the binding energy of *Oid* very accurately.

of roughly  $2 k_B T$ .

The dependence of our fits on the choice of data points included is also revealed in fig. 28. In this case, we show the result of using eqn. 4 as the basis of the fit and including different subsets of the data from fig. 3.

## 5.5 Individual Looped States

In figs. 24 and 25 we showed the looping probabilities corresponding to each individual loop: the bottom and middle loops. In order to analyze these results we can construct an individual loop ratio analogous to the one defined in eqn. 4. For the case of the bottom loop, for example, this is

$$p_{\text{ratio,B}} = \frac{p_{\text{loop,B}}}{p_{\text{unloop}}} = \frac{4K_1}{J_{\text{loop,B}}} + \frac{4[R]}{J_{\text{loop,B}}}. \quad (23)$$

Using an approach analogous to the one leading to eqn. 5 we obtain the looping  $J$  factors associated with each individual loop as shown in fig. 29. In fig. 30 we show their corresponding looping energies.

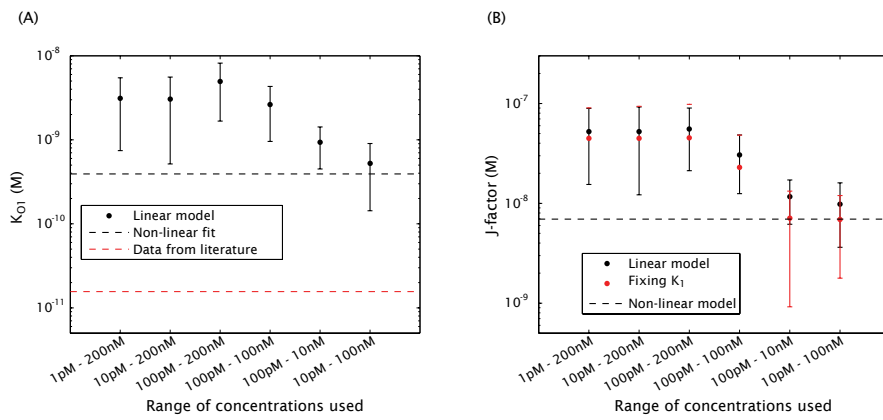


Figure 27: Sensitivity of fits to the method of data analysis. (A) Different fits to the value of  $K_1$  using the linear model of eqn. 4 and different ranges of data points from fig. 3. The results corresponding to the non-linear model of eqn. 20 are also shown. (B) Different fits to the value of  $J_{loop}$  using the linear and non-linear models as shown in (A). “Fixing  $K_1$ ” corresponds to fixing the  $O1$  dissociation constant to the literature value shown in table 1.

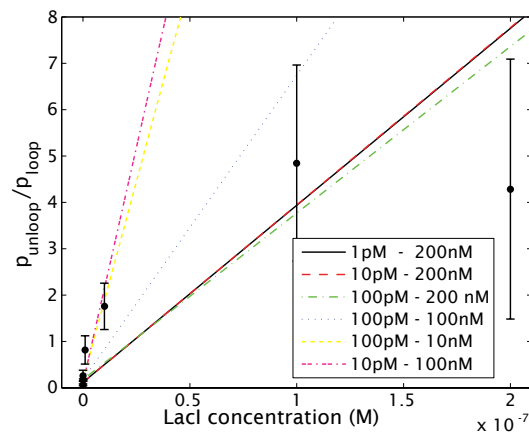


Figure 28: Sensitivity of linear fits to the range of data used. Different ranges of concentration from fig. 3 are fit using the linear model of eqn. 4.

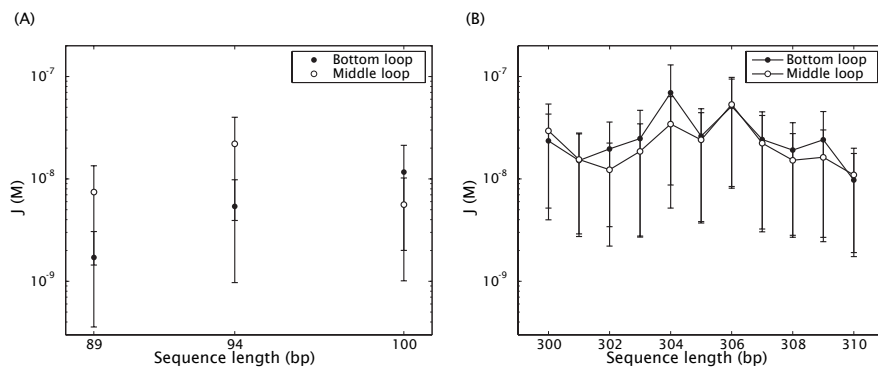


Figure 29: Individual loops  $J_{loop}$  as a function of sequence length. (A) Results for short constructs, (B) results for long constructs.

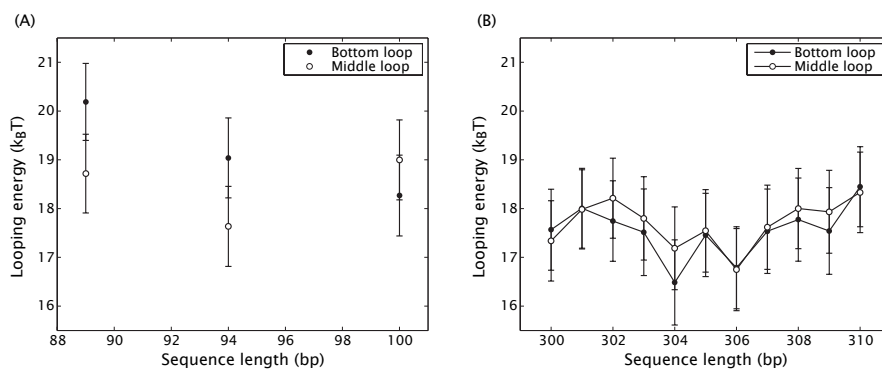


Figure 30: Individual loops energies as a function of sequence length. (A) Results for short constructs, (B) results for long constructs.

## 5.6 Monte Carlo simulation

Our mathematical model built on our previous work [75, 80, 101], which showed that a Gaussian-sampling simulation could accurately model the experimentally observed relation between DNA tether length and TPM bead motion by including an effective entropic stretching force from bead-wall repulsion. This technique is essentially a Monte Carlo evaluation of the equilibrium partition function of a chain. Instead of a Metropolis implementation, we simply generated many discretized chains using Gaussian distributions for each link’s bending and twisting angles, then discarded any such chains that violated the global steric constraints. To compute looping  $J$  factors, we modified our previous code to monitor the separation and relative orientation of the operator centers in the generated chains, and found the fraction of all chains that met the conditions needed for looping. See [41] for more details.

To obtain the distributions of bead excursion shown in fig. 10, we needed to make a correction before comparing to the experimental data. Our video camera gathers light for almost the entire 33 ms video frame time. This time scale is an appreciable fraction of the bead’s diffusion time in the trap created by its tether, leading to a blurring of the bead image and an apparent reduction of bead RMS excursion. We measured this effect by looking at the apparent RMS excursion for a bead/tether system with many different shutter times, then corrected our numerically generated values for the position of the bead center to account for blurring [41].

In addition, we reduced our simulation data in a way that parallels what was done with the experimental data. The experiment takes data in the form of a time series for the projected location of the bead center (relative to its attachment), that is,  $(x(t), y(t))$ . We found the length-squared of these position vectors,  $R^2$ , then applied a Gaussian filter that essentially averaged over a 4-s window. To simulate equilibrium averages in this context, we harvested batches of  $N_{\text{samp}}$  independent simulated chains and found the standard deviation of excursion within each batch. From the resulting series of values for  $R_{\text{RMS}} = \sqrt{\langle R^2 \rangle_{N_{\text{samp}}}}$ , we made a histogram representing the probability density function of  $R_{\text{RMS}}$ . To choose an appropriate value for  $N_{\text{samp}}$ , we found a characteristic time scale for bead diffusion from the time autocorrelation function of  $R_{\text{RMS}}$ , then divided the 4 s window into  $N_{\text{samp}}$  slots corresponding to the larger of the frame time, 33 ms, or the bead diffusion time [41].

## References

- [1] Garcia HG, Grayson P, Han L, Inamdar M, Kondev J, et al. (2007) Biological consequences of tightly bent DNA: The other life of a macromolecular celebrity. *Biopoly-*

- mers 85:115–30.
- [2] Segal E, Fondufe-Mittendorf Y, Chen L, Thastrom A, Field Y, et al. (2006) A genomic code for nucleosome positioning. *Nature* 442:772–8.
  - [3] Cloutier TE, Widom J (2004) Spontaneous sharp bending of double-stranded DNA. *Mol Cell* 14:355–62.
  - [4] Adhya S (1989) Multipartite genetic control elements: communication by DNA loop. *Annu Rev Genet* 23:227–50.
  - [5] Schleif R (1992) DNA looping. *Annu Rev Biochem* 61:199–223.
  - [6] Matthews KS (1992) DNA looping. *Microbiol Rev* 56:123–36.
  - [7] Zeller RW, Griffith JD, Moore JG, Kirchhamer CV, Britten RJ, et al. (1995) A multimerizing transcription factor of sea urchin embryos capable of looping DNA. *Proc Natl Acad Sci U S A* 92:2989–93.
  - [8] Loh YH, Wu Q, Chew JL, Vega VB, Zhang W, et al. (2006) The Oct4 and Nanog transcription network regulates pluripotency in mouse embryonic stem cells. *Nat Genet* 38:431–40.
  - [9] Wei CL, Wu Q, Vega VB, Chiu KP, Ng P, et al. (2006) A global map of p53 transcription-factor binding sites in the human genome. *Cell* 124:207–19.
  - [10] Dunn TM, Hahn S, Ogden S, Schleif RF (1984) An operator at -280 base pairs that is required for repression of araBAD operon promoter: addition of DNA helical turns between the operator and promoter cyclically hinders repression. *Proc Natl Acad Sci USA* 81:5017–20.
  - [11] Ptashne M (2004) A genetic switch: phage lambda revisited. Cold Spring Harbor, N.Y.: Cold Spring Harbor Laboratory Press, 3rd edition.
  - [12] Müller-Hill B (1996) The *lac* Operon: a short history of a genetic paradigm. Berlin; New York: Walter de Gruyter.
  - [13] Müller J, Oehler S, Müller-Hill B (1996) Repression of *lac* promoter as a function of distance, phase and quality of an auxiliary *lac* operator. *J Mol Biol* 257:21–9.
  - [14] Becker NA, Kahn JD, Maher III LJ (2005) Bacterial repression loops require enhanced DNA flexibility. *J Mol Biol* 349:716–30.

- [15] Becker NA, Kahn JD, Maher r L J (2007) Effects of nucleoid proteins on DNA repression loop formation in *escherichia coli*. *Nucleic Acids Res* 35:3988–4000.
- [16] Schafer DA, Gelles J, Sheetz MP, Landick R (1991) Transcription by single molecules of RNA polymerase observed by light microscopy. *Nature* 352:444–8.
- [17] Yin H, Landick R, Gelles J (1994) Tethered particle motion method for studying transcript elongation by a single RNA polymerase molecule. *Biophys J* 67:2468–78.
- [18] Vanzi F, Vladimirov S, Knudsen CR, Goldman YE, Cooperman BS (2003) Protein synthesis by single ribosomes. *RNA* 9:1174–9.
- [19] Pouget N, Dennis C, Turlan C, Grigoriev M, Chandler M, et al. (2004) Single-particle tracking for DNA tether length monitoring. *Nucleic Acids Res* 32:e73.
- [20] Blumberg S, Tkachenko AV, Meiners JC (2005) Disruption of protein-mediated DNA looping by tension in the substrate DNA. *Biophys J* 88:1692–701.
- [21] Pouget N, Turlan C, Destainville N, Salome L, Chandler M (2006) Is911 transpososome assembly as analysed by tethered particle motion. *Nucleic Acids Res* 34:4313–23.
- [22] van den Broek B, Vanzi F, Normanno D, Pavone FS, Wuite GJ (2006) Real-time observation of DNA looping dynamics of Type III restriction enzymes NaeI and NarI. *Nucleic acids research* 34:167–174.
- [23] Tolic-Norrelykke SF, Rasmussen MB, Pavone FS, Berg-Sorensen K, Oddershede LB (2006) Stepwise bending of DNA by a single TATA-box binding protein. *Biophys J* 90:3694–703.
- [24] Guerra RF, Imperadori L, Mantovani R, Dunlap DD, Finzi L (2007) DNA compaction by the nuclear factor-Y. *Biophys J* 93:176–82.
- [25] Finzi L, Gelles J (1995) Measurement of lactose repressor-mediated loop formation and breakdown in single DNA molecules. *Science* 267:378–80.
- [26] Vanzi F, Broggio C, Sacconi L, Pavone FS (2006) Lac repressor hinge flexibility and DNA looping: single molecule kinetics by tethered particle motion. *Nucleic Acids Res* 34:3409–20.
- [27] Zurla C, Franzini A, Galli G, Dunlap DD, Lewis DEA, et al. (2006) Novel tethered particle motion analysis of cI protein-mediated DNA looping in the regulation of bacteriophage lambda. *Journal of Physics-Condensed Matter* 18:S225–S234.

- [28] Wong OK, Guthold M, Erie DA, Gelles J (2008). Interconvertible lactose repressor-DNA looped complexes revealed by single-molecule experiments. Submitted to PLoS Biology.
- [29] Zurla C, Samuely T, Bertoni G, Valle F, Dietler G, et al. (2007) Integration host factor alters LacI-induced DNA looping. *Biophys Chem* 128:245–52.
- [30] Normanno D, Vanzi F, Pavone FS (2008) Single-molecule manipulation reveals supercoiling-dependent modulation of *lac* repressor-mediated DNA looping. *Nucleic Acids Res* 36:2505–13.
- [31] Krämer H, Niemöller M, Amouyal M, Revet B, von Wilcken-Bergmann B, et al. (1987) *Lac* repressor forms loops with linear DNA carrying two suitably spaced *lac* operators. *EMBO J* 6:1481–91.
- [32] Hsieh WT, Whitson PA, Matthews KS, Wells RD (1987) Influence of sequence and distance between two operators on interaction with the *lac* repressor. *J Biol Chem* 262:14583–91.
- [33] Krämer H, Amouyal M, Nordheim A, Müller-Hill B (1988) DNA supercoiling changes the spacing requirement of two *lac* operators for DNA loop formation with *lac* repressor. *EMBO J* 7:547–56.
- [34] Whitson PA, Hsieh WT, Wells RD, Matthews KS (1987) Influence of supercoiling and sequence context on operator DNA binding with *lac* repressor. *J Biol Chem* 262:14592–9.
- [35] Borowiec JA, Zhang L, Sasse-Dwight S, Gralla JD (1987) DNA supercoiling promotes formation of a bent repression loop in *lac* DNA. *J Mol Biol* 196:101–11.
- [36] Cloutier TE, Widom J (2005) DNA twisting flexibility and the formation of sharply looped protein-DNA complexes. *Proc Natl Acad Sci U S A* 102:3645–50.
- [37] Zhang Y, McEwen AE, Crothers DM, Levene SD (2006) Statistical-mechanical theory of DNA looping. *Biophys J* 90:1903–12.
- [38] Swigon D, Coleman BD, Olson WK (2006) Modeling the Lac repressor-operator assembly: The influence of DNA looping on Lac repressor conformation. *Proc Natl Acad Sci U S A* 103:9879–84.
- [39] Geanacopoulos M, Vasmatzis G, Zhurkin VB, Adhya S (2001) Gal repressosome contains an antiparallel DNA loop. *Nat Struct Biol* 8:432–6.

- [40] Balaeff A, Mahadevan L, Schulten K (2006) Modeling DNA loops using the theory of elasticity. *Phys Rev E Stat Nonlin Soft Matter Phys* 73:031919.
- [41] Towles K, Beausang JF, Garcia HG, Phillips R, Nelson PC First-principles calculation of DNA looping in tethered particle experiments. In preparation; to appear on [ArXiv.org](http://ArXiv.org).
- [42] Ackers GK, Johnson AD, Shea MA (1982) Quantitative model for gene regulation by lambda phage repressor. *Proc Natl Acad Sci U S A* 79:1129–33.
- [43] Buchler NE, Gerland U, Hwa T (2003) On schemes of combinatorial transcription logic. *Proc Natl Acad Sci U S A* 100:5136–41.
- [44] Bintu L, Buchler NE, Garcia HG, Gerland U, Hwa T, et al. (2005) Transcriptional regulation by the numbers: models. *Curr Opin Genet Dev* 15:116–24.
- [45] Bintu L, Buchler NE, Garcia HG, Gerland U, Hwa T, et al. (2005) Transcriptional regulation by the numbers: applications. *Curr Opin Genet Dev* 15:125–35.
- [46] Motion of the bead is systematically characterized with various DNA lengths ranging from 200bp to 3 kbp. Such DNA is then interpolated using a second order polynomial function to served as a calibration curve. From this curve, for any given length DNA tether in that range, the amplitude of the motion of the DNA tethered bead can be evaluated.
- [47] Friedman AM, Fischmann TO, Steitz TA (1995) Crystal structure of *lac* repressor core tetramer and its implications for DNA looping. *Science* 268:1721–7.
- [48] Mehta RA, Kahn JD (1999) Designed hyperstable Lac repressor. DNA loop topologies suggest alternative loop geometries. *J Mol Biol* 294:67–77.
- [49] Semsey S, Tolstorukov MY, Virnik K, Zhurkin VB, Adhya S (2004) DNA trajectory in the gal repressosome. *Genes Dev* 18:1898–907.
- [50] Levandoski MM, Tsodikov OV, Frank DE, Melcher SE, Saecker RM, et al. (1996) Cooperative and anticooperative effects in binding of the first and second plasmid Osym operators to a LacI tetramer: evidence for contributions of non-operator DNA binding by wrapping and looping. *J Mol Biol* 260:697–717.
- [51] Barry JK, Matthews KS (1999) Thermodynamic analysis of unfolding and dissociation in lactose repressor protein. *Biochemistry* 38:6520–8.



- [52] Saiz L, Rubi JM, Vilar JM (2005) Inferring the *in vivo* looping properties of DNA. Proc Natl Acad Sci U S A 102:17642–5.
- [53] deHaseth PL, Gross CA, Burgess RR, Record J M T (1977) Measurement of binding constants for protein-DNA interactions by DNA-cellulose chromatography. Biochemistry 16:4777–83.
- [54] O’Gorman RB, Dunaway M, Matthews KS (1980) DNA binding characteristics of lactose repressor and the trypsin-resistant core repressor. J Biol Chem 255:10100–6.
- [55] Revzin A, von Hippel PH (1977) Direct measurement of association constants for the binding of *escherichia coli lac* repressor to non-operator DNA. Biochemistry 16:4769–76.
- [56] Record J M T, deHaseth PL, Lohman TM (1977) Interpretation of monovalent and divalent cation effects on the *lac* repressor-operator interaction. Biochemistry 16:4791–6.
- [57] Kao-Huang Y, Revzin A, Butler AP, O’Conner P, Noble DW, et al. (1977) Nonspecific DNA binding of genome-regulating proteins as a biological control mechanism: measurement of DNA-bound *escherichia coli lac* repressor *in vivo*. Proc Natl Acad Sci U S A 74:4228–32.
- [58] Wang AC, Revzin A, Butler AP, von Hippel PH (1977) Binding of *E. coli lac* repressor to non-operator DNA. Nucleic Acids Res 4:1579–93.
- [59] Barkley MD (1981) Salt dependence of the kinetics of the *lac* repressor-operator interaction: role of nonoperator deoxyribonucleic acid in the association reaction. Biochemistry 20:3833–42.
- [60] Zhang X, Gottlieb PA (1993) Thermodynamic and alkylation interference analysis of the *lac* repressor-operator substituted with the analogue 7-deazaguanine. Biochemistry 32:11374–84.
- [61] Mossing MC, Record J M T (1985) Thermodynamic origins of specificity in the *lac* repressor-operator interaction. adaptability in the recognition of mutant operator sites. J Mol Biol 186:295–305.
- [62] Horton N, Lewis M, Lu P (1997) *Escherichia coli lac* repressor-*lac* operator interaction and the influence of allosteric effectors. J Mol Biol 265:1–7.

- [63] Goeddel DV, Yansura DG, Caruthers MH (1977) Binding of synthetic lactose operator DNAs to lactose repressors. *Proc Natl Acad Sci U S A* 74:3292–6.
- [64] Falcon CM, Matthews KS (1999) Glycine insertion in the hinge region of lactose repressor protein alters DNA binding. *J Biol Chem* 274:30849–57.
- [65] Winter RB, von Hippel PH (1981) Diffusion-driven mechanisms of protein translocation on nucleic acids. 2. The *escherichia coli* repressor–operator interaction: equilibrium measurements. *Biochemistry* 20:6948–60.
- [66] Saiz L, Vilar JM (2006) DNA looping: the consequences and its control. *Curr Opin Struct Biol* 16:344–50.
- [67] Frank DE, Saecker RM, Bond JP, Capp MW, Tsodikov OV, et al. (1997) Thermodynamics of the interactions of *lac* repressor with variants of the symmetric *lac* operator: effects of converting a consensus site to a non-specific site. *J Mol Biol* 267:1186–206.
- [68] Lee DH, Schleif RF (1989) *In vivo* DNA loops in araCBAD: size limits and helical repeat. *Proc Natl Acad Sci U S A* 86:476–80.
- [69] Law SM, Bellomy GR, Schlax PJ, Record J M T (1993) *In vivo* thermodynamic analysis of repression with and without looping in *lac* constructs. estimates of free and local *lac* repressor concentrations and of physical properties of a region of supercoiled plasmid DNA *in vivo*. *J Mol Biol* 230:161–73.
- [70] Shore D, Baldwin RL (1983) Energetics of DNA twisting. I. Relation between twist and cyclization probability. *J Mol Biol* 170:957–81.
- [71] Du Q, Smith C, Shiffeldrim N, Vologodskaja M, Vologodskii A (2005) Cyclization of short DNA fragments and bending fluctuations of the double helix. *Proc Natl Acad Sci U S A* 102:5397–402.
- [72] Record MT, Mazur S, Melancon P, Roe JH, Shaner SL, et al. (1981) Double helical DNA: conformations, physical properties, and interactions with ligands. *Annual review of biochemistry* 50:997–1024.
- [73] Strick T, Allemand J, Croquette V, Bensimon D (2000) Twisting and stretching single DNA molecules. *Progress in biophysics and molecular biology* 74:115–40.
- [74] Moroz JD, Nelson P (1998) Entropic elasticity of twist-storing polymers. *Macromolecules* 31:6333–6347.

- [75] Segall DE, Nelson PC, Phillips R (2006) Volume-exclusion effects in tethered-particle experiments: Bead size matters. *Physical Review Letters* 96:088306–(1–4).
- [76] Yan J, Marko JF (2004) Localized single-stranded bubble mechanism for cyclization of short double helix DNA. *Phys Rev Lett* 93:108108–(1–4).
- [77] Wiggins PA, Nelson PC, Phillips R (2005) Exact theory of kinkable elastic polymers. *Phys Rev E* 71:021909–(1–19).
- [78] Nelson PC, Zurla C, Brogioli D, Beausang JF, Finzi L, et al. (2006) Tethered particle motion as a diagnostic of DNA tether length. *J Phys Chem B* 110:17260–7.
- [79] Czapla L, Swigon D, Olson WK (2006) Sequence-dependent effects in the cyclization of short DNA. *Journal of Chemical Theory and Computation* 2:685–695.
- [80] Nelson PC (2007) Colloidal particle motion as a diagnostic of DNA conformational transitions. *Curr Op Colloid Intef Sci* 12:307–313.
- [81] Lewis M, Chang G, Horton NC, Kercher MA, Pace HC, et al. (1996) Crystal structure of the lactose operon repressor and its complexes with DNA and inducer. *Science* 271:1247–54.
- [82] Strick TR, Croquette V, Bensimon D (1998) Homologous pairing in stretched supercoiled DNA. *Proc Natl Acad Sci USA* 95:10579–10583.
- [83] Wang MD, Yin H, Landick R, Gelles J, Block SM (1997) Stretching DNA with optical tweezers. *Biophys J* 72:1335–1346.
- [84] Villa E, Balaeff A, Schulten K (2005) Structural dynamics of the *lac* repressor-DNA complex revealed by a multiscale simulation. *Proc Natl Acad Sci U S A* 102:6783–8.
- [85] Wiggins PA, Van der Heijden T, Moreno-Herrero F, Spakowitz A, Phillips R, et al. (2006) High flexibility of DNA on short length scales probed by atomic force microscopy. *Nature Nanotech* 1:137–141.
- [86] Ruben GC, Roos TB (1997) Conformation of *lac* repressor tetramer in solution, bound and unbound to operator DNA. *Microsc Res Tech* 36:400–16.
- [87] Edelman LM, Cheong R, Kahn JD (2003) Fluorescence resonance energy transfer over approximately 130 basepairs in hyperstable Lac repressor-DNA loops. *Biophys J* 84:1131–45.

- [88] Morgan MA, Okamoto K, Kahn JD, English DS (2005) Single-molecule spectroscopic determination of Lac repressor-DNA loop conformation. *Biophys J* 89:2588–96.
- [89] Zhang Y, McEwen AE, Crothers DM, Levene SD (2006) Analysis of *in-vivo* LacR-mediated gene repression based on the mechanics of DNA looping. *PLoS ONE* 1:e136.
- [90] Oehler S, Amouyal M, Kolkhof P, von Wilcken-Bergmann B, Müller-Hill B (1994) Quality and position of the three *lac* operators of *E. coli* define efficiency of repression. *EMBO J* 13:3348–55.
- [91] Lutz R, Bujard H (1997) Independent and tight regulation of transcriptional units in *Escherichia coli* via the LacR/O, the TetR/O and AraC/I1-I2 regulatory elements. *Nucleic Acids Res* 25:1203–10.
- [92] Rosenfeld N, Young JW, Alon U, Swain PS, Elowitz MB (2005) Gene regulation at the single-cell level. *Science* 307:1962–5.
- [93] Oehler S, Eismann ER, Kramer H, Muller-Hill B (1990) The three operators of the *lac* operon cooperate in repression. *EMBO J* 9:973–9.
- [94] Gelles J, Schnapp B, Sheetz M (1988) Tracking kinesin-driven movements with nanometre-scale precision. *Nature* 331:450–453.
- [95] Colquhoun D, Sigworth FJ (1995) Fitting and statistical analysis of single-channel records. In: Sakmann B, Neher E, editors, *Single-Channel Recording*, New York: Plenum Press. Second edition, pp. 483–587.
- [96] Beausang JF, Zurla C, Manzo C, Dunlap D, Finzi L, et al. (2007) DNA looping kinetics analyzed using diffusive hidden Markov model. *Biophysical journal* 92:L64–6.
- [97] Beausang JF, Nelson PC (2007) Diffusive hidden Markov model characterization of DNA looping dynamics in tethered particle experiments. *Physical Biology* 4:205–219.
- [98] Falcon CM, Swint-Kruse L, Matthews KS (1997) Designed disulfide between N-terminal domains of lactose repressor disrupts allosteric linkage. *The Journal of biological chemistry* 272:26818–21.
- [99] Phillips R, Kondev J, Theriot J (2008) *Physical Biology of the Cell, in press*. New York: Garland Science.
- [100] Shore D, Langowski J, Baldwin RL (1981) DNA flexibility studied by covalent closure of short fragments into circles. *Proc Natl Acad Sci U S A* 78:4833–7.

- [101] Nelson PC, Zurla C, Brogioli D, Beausang JF, Finzi L, et al. (2006) Tethered particle motion as a diagnostic of DNA tether length. *Journal of Physical Chemistry B* 110:17260–17267.